Interaction Notes

Note 363

July 1977

Numerical Electromagnetic Code (NEC) Method of Moments Volume I - Program Description Theory

G. J. Burke
A. J. Poggio

Lawrence Livermore Laboratory
Livermore, California

Abstract

The Numerical Electromagnetics Code (NEC-(1,2)A) is a computer code for analyzing the electromagnetic response of an arbitrary structure consisting of wires and surfaces in free space or over a ground plane. The analysis is accomplished by the numerical solution of integral equations for induced currents. The excitation may be an incident plane wave or a voltage source on a wire while the output may include current and charge density, electric or magnetic field in the vicinity of the structure, and radiated fields. Hence, the code may be used for antenna analysis, EMP, or scattering studies.

Volume I of the document includes the equations on which the code is based and a discussion of the approximations and numerical methods used in the numerical solution. Some comparisons to demonstrate the range of accuracy of approximations are also included. Details of the coding and a User's Guide are to be provided as Volumes II and III.

Preface

The Numerical Electromagnetics Code (NEC(1,2)A) has been developed at the Lawrence Livermore Laboratory, Livermore, California, under the sponsorship of the Naval Ocean Systems Center and the Air Force Weapons Laboratory. It is an advanced version of the Antenna Modeling Program (AMP) developed in the early 1979's by MBAssociates for the Naval Research Laboratory, Naval Ship Engineering Center, U.S. Army ECOM/ Communications Systems, U.S. Army Strategic Communications Command, and Rome Air Development Center under Office of Naval Research Contract N00014-71-C-0187. The present version of NEC is the result of efforts by G. J. Burke and A. J. Poggio of Lawrence Livermore Laboratory.

The documentation for NEC consists of three volumes:

Volume I: NEC(1,2)A Program Description - Theory, Interaction Note 363,

Volume II: NEC(1,2)A Program Description - Code, Interaction Application Memo 31, July 1977

Volume III: NEC(1,2)A User's Guide, Interaction Application Memo 32, July 1977

The documentation has been prepared by using the AMP documents as foundations and by modifying those as needed. In some cases this led to minor changes in the original documents while in many cases major modifications were required.

Over the years many individuals have been contributors to AMP and NEC(1,2)A and are acknowledged here as follows:

R. W. Adams	E. K. Miller
G. J. Burke	J. B. Morton
F. J. Deadrick	G. M. Pjerrou
K. K. Hazard	A. J. Poggio
D. L. Knepp	E. S. Selden

The support for the development of NEC(1,2)A at the Lawrence Livermore

MIPR-N0095376MP and the Air Force Weapons Laboratory under Project Order 76-090.

Cognizant individuals under who this project was carried out include:

J. Rockway, J. Logan, J. P. Castillo and MSgt. H. Goodwin.

Contents

Section		Page
I.	INTRODUCTION	6
II.	INTEGRAL EQUATION FORMULATION	8
	1. Electric Field Integral Equation (EFIE)	8
	2. Magnetic Field Integral Equation (MFIE)	11
	3. The EFIE-MFIE Hybrid Equation	12
	4. The Effect of a Ground Plane	14
III.	NUMERICAL SOLUTION	25
	1. Current Expansion on Wires	26
	2. Current Expansion on Surfaces	34
	3. The Matrix Equation for Current	36
	4. Solution of the Matrix Equation	37
IV.	MODELING OF ANTENNAS	43
	1. Source Modeling	43
	2. Nonradiating Networks	48
	3. Transmission Line Modeling	53
	4. Lumped or Distributed Loading	55
	5. Radiated Field Calculation	56
	6. Ground-Wave Field	59
V.	VALIDATING RESULTS	61
	1. Antennas over Ground	61
	2. Cylinder with Attached Wires	63
REFERENCES		72
APPENDIX		75

Illustrations

Figure		Page
1.	Plane-Wave Reflection at an Interface	20
2.	Current Basis Functions and Sum on a Four Segment Wire	29
3.	Segments Covered by the i^{th} Basis Function	29
4.	Detail of the Connection of a Wire to a Surface	36
5.	Biconical Transmission Line Model of Source Region	45
6.	Field Plots for a Linear Dipole, Ω = 15	48
7.	Voltage and Current Reference Directions at Network Ports	50
8.	Network Connection to Segments	50
9.	Network Port and Voltage Source Connected to a Segment	51
10.	Current Distribution on a Two-Wire Transmission Line from NEC Compared with the Ideal Transmission Line Solution	54
11.	Input Resistance of a Half-Wave Dipole Over a Lossy Ground at 3 MHz.	62
12.	Input Resistance of a Horizontal Dipole, 1λ Long, Located a Distance H above a Purely Dielectric Ground (Dielectric Constant ε_r).	63
13.	Input Resistance of a Horizontal Half-Wave Dipole Located a Distance h above a Purely Dielectric Ground, ε_r = s	64
14.	Radiation Patterns (Linear Voltage Scale) of a Monopole over a Dielectric Ground	65
15.	Input Impedance and Radiation Patterns for a Parasitic Array of Two Half-Wave Dipoles	66
16.	Input Resistance for a Parasitic Array of Two Half-Wave Dipoles	67
17.	Experimental/Numerical Radiation Pattern of Cylinder with Attached Wires	68
18.	Experimental/Numerical Radiation Pattern of Cylinder with Attached Wires	69
19.	Experimental/Numerical Radiation Pattern of Cylinder with Attached Wires	70
20.	Segmentation of Cylinder for Wires Connected to End and Side	71
A1.	Current-Filament Geometry for the Thin-Wire Kernel	76
A2.	Current Geometry for the Extended Thin-Wire Kernel	78

Section I
Introduction

The Numerical Electromagnetics Code (NEC-(1,2)A)* is a user-oriented computer code for the analysis of the electromagnetic response of antennas and other metal structures. It is built around the numerical solution of integral equations for the currents induced on the structure by sources or incident fields. This approach avoids many of the simplifying assumptions required by other solution methods and provides a highly accurate and versatile tool for electromagnetic analysis.

The code combines an integral equation for smooth surfaces with one specialized to wires to provide for convenient and accurate modeling of a wide range of structures. A model may include nonradiating networks and transmission lines connecting parts of the structure, perfect or imperfect conductors, and lumped-element loading. A structure may also be modeled over a ground plane that may be either a perfect or imperfect conductor.

The excitation may be either voltage sources on the structure or an incident plane wave of linear or elliptic polarization. The output may include induced currents and charges, near electric or magnetic fields, and radiated fields. Hence, the program is suited to either antenna analysis or scattering and EMP studies.

The integral-equation approach is best suited to structures with dimensions up to several wavelengths. Although there is no theoretical size limit, the numerical solution requires a matrix equation of increasing order as the structure size is increased relative to wavelength. Hence, modeling very large structures may require more computer time and file storage than is practical on a particular machine. In such cases standard high-frequency approximations such as geometrical or physical optics, or geometric theory of diffraction may be more suitable than the integral equation approach used in NEC.

The code NEC is the latest in a series of electromagnetics codes, each of which has built upon the previous one. The first in the series was the code BRACT which was developed at MBAssociates in San Ramon, California, under the funding of the Air Force Space and Missiles Systems Organization (refs. 1 and 2). BRACT was specialized to scattering by arbitrary thin-wire configurations.

*NEC-(1,2)A will be abbreviated to NEC elsewhere in this report.

The code AMP followed BRACT and was developed at MBAssociates with funding from the Naval Research Laboratory, Naval Ship Engineering Center, U.S. Army ECOM/Communications Systems, U.S. Army Strategic Communications Command, and Rome Air Development Center under Office of Naval Research Contract N00014-71-C-0187. AMP uses the same numerical solution method as BRACT with the addition of the capability of modeling a structure over a ground plane and an option to use file storage to greatly increase the maximum structure size that may be modeled. The program input and output were extensively revised for AMP so that the code could be used with a minimum of learning and computer programming experience. AMP includes extensive documentation to aid in understanding, using, and modifying the code (refs. 3, 4 and 5).

A modeling option specialized to surfaces was added to the wire modeling capabilities of AMP in the AMP2 code (ref. 6). A simplified approximation for large interaction distances was also included in AMP2 to reduce running time for large structures.

The code NEC added to AMP2 a more accurate current expansion along wires and at multiple wire junctions, and an option in the wire modeling technique for greater accuracy on thick wires. A new model for a voltage source was added and several other modifications made for increased accuracy and efficiency.

Part I of this document describes the equations and numerical methods used in NEC. Part III: NEC User's Guide (ref. 7) contains instructions for using the code, including preparation of input and interpretation of output. Part II: NEC Program Description — Code (ref. 8) describes the coding in detail. The user encountering the code for the first time should begin with the User's Guide and try modeling some simple antennas. Part II will be of interest mainly to someone attempting to modify the code. Reading part I will be useful to the new user of NEC however, since an understanding of the theory and solution method will assist in the proper application of the code.

Section II
Integral Equation Formulation

The NEC program uses both an electric-field integral equation (EFIE) and a magnetic-field integral equation (MFIE) to model the electromagnetic response of general structures. Each equation has advantages for particular structure types. The EFIE is well suited for thin-wire structures of small or vanishing conductor volume while the MFIE, which fails for the thin-wire case, is more attractive for voluminous structures, especially those having large smooth surfaces. The EFIE can also be used to model surfaces and is preferred for thin structures where there is little separation between a front and back surface. Although the EFIE is specialized to thin wires in this program, it has been used to represent surfaces by wire grids with reasonable success for far-field quantities but with variable accuracy for surface fields. For a structure containing both wires and surfaces the EFIE and MFIE are coupled. This combination of the EFIE and MFIE was proposed and used by Albertsen, Hansen, and Jensen at the Technical University of Denmark (ref. 9) although the details of their numerical solution differ from those in NEC. A rigorous derivation of the EFIE and MFIE used in NEC is given by Poggio and Miller (ref. 10). The equations and their derivation are outlined in the following sections.

1. THE ELECTRIC FIELD INTEGRAL EQUATION (EFIE)

The form of the EFIE used in NEC follows from an integral representation for the electric field of a volume current distribution $\vec{J}$,

$$\vec{E}(\vec{r}) = \frac{-j\eta}{4\pi k} \int_V \vec{J}(\vec{r}') \cdot \overline{\overline{G}}(\vec{r}, \vec{r}')\, dV', \qquad (1)$$

where

$$\overline{\overline{G}}(\vec{r}, \vec{r}') = (k^2\overline{\overline{I}} + \nabla\nabla)g(\vec{r}, \vec{r}'),$$

$$g(\vec{r}, \vec{r}') = \exp(-jk|\vec{r} - \vec{r}'|)/|\vec{r} - \vec{r}'|,$$

$$k = \omega\sqrt{\mu_o \varepsilon_o},$$

$$\eta = \sqrt{\mu_o/\varepsilon_o}$$

and the time convention is $\exp(j\omega t)$. $\overline{\overline{I}}$ is the identity dyad $(\hat{x}\hat{x} + \hat{y}\hat{y} + \hat{z}\hat{z})$. When the current distribution is limited to the surface of a perfectly conducting body, equation (1) becomes

$$\vec{E}(\vec{r}) = \frac{-j\eta}{4\pi k} \int_S \vec{J}_s(\vec{r}') \cdot \overline{\overline{G}}(\vec{r}, \vec{r}')\, dA', \tag{2}$$

with $\vec{J}_s$ the surface current density. The observation point $\vec{r}$ is restricted to be off the surface S so that $\vec{r} \neq \vec{r}'$.

If $\vec{r}$ approaches S as a limit, equation (2) becomes

$$\vec{E}(\vec{r}) = \frac{-j\eta}{4\pi k} \oint_S \vec{J}_s(\vec{r}') \cdot \overline{\overline{G}}(\vec{r}, \vec{r}')\, dA', \tag{3}$$

where the principal value integral, $\oint$, is indicated since $g(\vec{r}, \vec{r}')$ is now unbounded.

An integral equation for the current induced on S by an incident field $\vec{E}^I$ can be obtained from equation (3) and the boundary condition for $\vec{r} \in S$,

$$\hat{n}(\vec{r}) \times \left[\vec{E}^s(\vec{r}) + \vec{E}^I(\vec{r}) \right] = 0, \tag{4}$$

where $\hat{n}(\vec{r})$ is the unit normal vector of the surface at $\vec{r}$ and $\vec{E}^s$ is the field due to the induced current $\vec{J}_s$. Substituting equation (3) for $\vec{E}^s$ yields the integral equation,

$$-\hat{n}(\vec{r}) \times \vec{E}^I(\vec{r}) = \frac{-j\eta}{4\pi k} \hat{n}(\vec{r}) \times$$

$$\oint_S \vec{J}_s(\vec{r}') \cdot (k^2 \overline{\overline{I}} + \nabla\nabla) g(\vec{r}, \vec{r}')\, dA'. \tag{5}$$

The vector integral in equation (5) can be reduced to a scalar integral equation when the conducting surface S is that of a cylindrical thin wire, thereby making the solution much easier. The assumptions applied for a thin wire, known as the thin-wire approximation, are as follows:

a. Transverse currents can be neglected relative to axial currents on the wire.

b. The circumferential variation in the axial current can be neglected.

c. The current can be represented by a filament on the wire axis.

d. The boundary condition on the electric field need be enforced in the axial direction only.

These widely used approximations are valid as long as the wire radius is much less than the wavelength and much less than the wire length. An alternate kernel for the EFIE, based on an extended thin-wire approximation in which condition c is relaxed, is also included in NEC for wires having too large a radius for the thin-wire approximation (ref. 11).

From assumptions a, b and c, the surface current $\vec{J}_s(\vec{r})$ on a wire of radius a can be replaced by a filamentary current I where

$$I(s)\hat{s} = 2\pi a\vec{J}_s(\vec{r}),$$

s = distance parameter along the wire axis at $\vec{r}$, and

$\hat{s}$ = unit vector tangent to the wire axis at $\vec{r}$.

Equation (5) then becomes

$$-\hat{n}(\vec{r}) \times \vec{E}^I(\vec{r}) = \frac{-j\eta}{4\pi k}\,\hat{n}(\vec{r}) \times \int_L I(s')\left(k^2\hat{s}' - \nabla\frac{\partial}{\partial s'}\right) g(\vec{r}, \vec{r}')\, ds', \qquad (6)$$

where the integration is over the length of the wire. Enforcing the boundary condition in the axial direction reduces Eq. (6) to the scalar equation,

$$-\hat{s} \cdot \vec{E}^I(\vec{r}) = \frac{-j\eta}{4\pi k}\int_L I(s')\left(k^2\hat{s}\cdot\hat{s}' - \frac{\partial^2}{\partial s\partial s'}\right) g(\vec{r}, \vec{r}')\, ds'. \qquad (7)$$

Since $\vec{r}'$ is now the point at s' on the wire axis while $\vec{r}$ is a point at s on the wire surface $|\vec{r} - \vec{r}'| \geq a$ and the integrand is bounded.

The accuracy of the thin-wire approximation for a segment of radius a and length Δ depends on ka and Δ/a. Studies have shown that the thin-wire approximation leads to errors of less than 1% for Δ/a greater than 8 (Ref. 11). Furthermore, in the numerical solution of the EFIE, the wire is divided into segments less than about 0.1λ in length to obtain an adequate representation

of current distribution thus restricting ka to less than about 0.08. The extended thin-wire approximation (ref. 11) is applicable to shorter and thicker segments, resulting in errors less than 1% for Δ/a greater than 2. In the extended thin-wire approximation, the current is assumed to be uniformly distributed around the wire circumference rather than concentrated in a filament on the axis. The field integral then involves an integration around the wire circumference. This integral is approximated by the first two terms in a series expansion in a^2, neglecting terms of order a^4. Thus, only the integration along the wire remains as with the thin-wire approximation.

The numerical solution used in NEC employs straight wire segments and a current that is the sum of constant, sin(ks), and cos(ks) components. The integrals along the wire can then be evaluated in closed form except for the integral for the field component parallel to a segment due to the constant current component. The field evaluation is thus greatly simplified for either the thin-wire or extended thin-wire kernel. The field expressions for both kernels are covered in the Appendix.

2. THE MAGNETIC FIELD INTEGRAL EQUATION (MFIE)

The MFIE is derived from the integral representation for the magnetic field of a surface current distribution $\vec{J}_s$,

$$\vec{H}^s(\vec{r}) = \frac{1}{4\pi} \int_S \vec{J}_s(\vec{r}') \times \nabla' \, g(\vec{r}, \vec{r}') \, dA', \tag{8}$$

where the differentiation is with respect to the integration variable $\vec{r}'$. If the current $\vec{J}_s$ is induced by an external incident field $\vec{H}^I$, then the total magnetic field inside the perfectly conducting surface must be zero. Hence, for $\vec{r}$ just inside the surface S,

$$\vec{H}^I(\vec{r}) + \vec{H}^s(\vec{r}) = 0, \tag{9}$$

where $\vec{H}^I$ is the incident field with the structure removed, and $\vec{H}^s$ is the scattered field given by equation (8). The integral equation for $\vec{J}_s$ may be obtained by letting $\vec{r}$ approach the surface point $\vec{r}_o$ from inside the surface along the normal $\hat{n}(\vec{r}_o)$. The surface component of equation (9) with equation (8) substituted for $\vec{H}^s$ is then

$$-\hat{n}(\vec{r}_o) \times \vec{H}^I(\vec{r}_o) = \hat{n}(\vec{r}_o) \times \frac{1}{4\pi} \lim_{\vec{r} \to \vec{r}_o} \int_S \vec{J}_s(\vec{r}') \times$$

$$\nabla' g(\vec{r}, \vec{r}') \, dA',$$

where $\hat{n}(\vec{r}_o)$ is the outward directed normal vector at $\vec{r}_o$. The limit can be evaluated by using a result of potential theory (ref. 12) to yield the integral equation

$$-\hat{n}(\vec{r}_o) \times \vec{H}^I(\vec{r}_o) = -\frac{1}{2} \vec{J}_s(\vec{r}_o) +$$

$$\frac{1}{4\pi} \oint_S \hat{n}(\vec{r}_o) \times \left[\vec{J}_s(\vec{r}') \times \nabla' g(\vec{r}_o, \vec{r}') \right] dA'. \qquad (10)$$

For solution in NEC, this vector integral equation is resolved into two scalar equations along the orthogonal surface vectors $\hat{t}_1$ and $\hat{t}_2$ where

$$\hat{t}_1(\vec{r}_o) \times \hat{t}_2(\vec{r}_o) = \hat{n}(\vec{r}_o).$$

By using the identity $\vec{u} \cdot (\vec{v} \times \vec{w}) = (\vec{u} \times \vec{v}) \cdot \vec{w}$ and noting that $\hat{t}_1 \times \hat{n} = -\hat{t}_2$ and $\hat{t}_2 \times \hat{n} = \hat{t}_1$, the scalar equations can be written,

$$\hat{t}_2(\vec{r}_o) \cdot \vec{H}^I(\vec{r}_o) = -\frac{1}{2} \hat{t}_1(\vec{r}_o) \cdot \vec{J}_s(\vec{r}_o) -$$

$$\frac{1}{4\pi} \oint_S \hat{t}_2(\vec{r}_o) \cdot \left[\vec{J}_s(\vec{r}') \times \nabla' g(\vec{r}_o, \vec{r}') \right] dA'; \qquad (11)$$

$$-\hat{t}_1(\vec{r}_o) \cdot \vec{H}^I(\vec{r}_o) = -\frac{1}{2} \hat{t}_2(\vec{r}_o) \cdot \vec{J}_s(\vec{r}_o) +$$

$$\frac{1}{4\pi} \oint_S \hat{t}_1(\vec{r}_o) \cdot \left[\vec{J}_s(\vec{r}') \times \nabla' g(\vec{r}_o, \vec{r}') \right] dA'. \qquad (12)$$

These two components suffice since there is no normal component of equation (10).

3. THE EFIE-MFIE HYBRID EQUATION

Program NEC uses the EFIE for thin wires and the MFIE for surfaces. For a structure consisting of both wires and surfaces, $\vec{r}$ in equation (7) is

restricted to the wires, with the integral for $E^s(\vec{r})$, extending over the complete structure. The thin-wire form of the integral in equation (7) is used over wires while the more general form of equation (5) must be used on surfaces. Likewise, $\vec{r}_o$ is restricted to surfaces in equations (11) and (12), with the integrals for $H^s(\vec{r})$ extending over the complete structure. On wires the integral is simplified by the thin-wire approximation. The resulting coupled integral equations are, for $\vec{r}$ on wire surfaces,

$$-\hat{s} \cdot \vec{E}^I(\vec{r}) = \frac{-j\eta}{4\pi k} \int_L I(s') \left(k^2 \hat{s} \cdot \hat{s}' - \frac{\partial^2}{\partial s \partial s'} \right) g(\vec{r},\vec{r}') \, ds'$$

$$- \frac{j\eta}{4\pi k} \int_{S_1} \vec{J}_s(\vec{r}) \cdot \left[k^2 \hat{s} - \nabla' \frac{\partial}{\partial s} \right] g(\vec{r},\vec{r}') \, dA', \qquad (13)$$

and for $\vec{r}$ on surfaces excluding wires

$$\hat{t}_2(\vec{r}) \cdot \vec{H}^I(\vec{r}) = - \frac{1}{4\pi} \hat{t}_2(\vec{r}) \cdot \int_L I(s') \left(\hat{s}' \times \nabla' \, g(\vec{r},\vec{r}') \right) ds'$$

$$- \frac{1}{2} \hat{t}_1(\vec{r}) \cdot \vec{J}_s(\vec{r}) -$$

$$\frac{1}{4\pi} \int\!\!\!\!\!\!- _{S_1} \hat{t}_2(\vec{r}) \cdot \left[\vec{J}_s(\vec{r}') \times \nabla' g(\vec{r},\vec{r}') \right] dA', \qquad (14)$$

and

$$-\hat{t}_1(\vec{r}) \cdot \vec{H}^I(\vec{r}) = \frac{1}{4\pi} \hat{t}_1(\vec{r}) \cdot \int_L I(s') \left(s' \times \nabla' g(\vec{r},\vec{r}') \right) ds'$$

$$- \frac{1}{2} \hat{t}_2(\vec{r}) \cdot \vec{J}_s(\vec{r}) +$$

$$\frac{1}{4\pi} \int\!\!\!\!\!\!- _{S_1} \hat{t}_1(\vec{r}) \cdot \left[\vec{J}_s(\vec{r}') \times \nabla' g(\vec{r},\vec{r}') \right] dA'. \qquad (15)$$

The symbol $\int_L$ represents integration over wires while $\int\!\!\!\!\!\!-_{S_1}$ represents integration over surfaces excluding wires. The numerical method used to solve equations (13), (14) and (15) is described in section III.

4. THE EFFECT OF A GROUND PLANE

A ground plane can change the electromagnetic response of a structure in three ways: (1) by modifying the current distribution through near-field interaction; (2) by changing the field illuminating the structure; and (3) by changing the reradiated field. Effects (2) and (3) are easily analyzed by plane-wave reflection as a direct ray and a ground-reflected ray. The reradiated field is not a plane wave when it reflects from the ground plane, but, as can be seen from reciprocity, plane-wave reflection formulas give the correct far-zone radiated field. Analysis of the near-field interaction effect is, however, more difficult than the other two effects. A rigorous solution for the near field was developed by Sommerfeld (ref. 13) but is cumbersome and lengthy, even for computer evaluation. The method used in NEC is an approximation based on the Fresnel plane-wave reflection coefficients (refs. 14 and 15). Although this approximation is inaccurate for structures very near to the ground, it provides a time-savings in NEC of up to two orders of magnitude, making possible the analysis of large structures that would be impractical with Sommerfeld's formulas. The range of validity of this reflection coefficient approximation is demonstrated in section V by comparison with results obtained with the Sommerfeld formulas.

Integral equations for the current on a conducting body over a ground plane can be developed in the same way as equations (13), (14), and (15) by replacing the free-space Green's functions by Green's functions for an infinite ground plane. The Green's functions for a ground plane, giving electric and magnetic fields at a point $\vec{r}$ due to an arbitrarily oriented infinitesimal current element at $\vec{r}'$ in the presence of a ground plane, were developed by Sommerfeld (ref. 13). For a vertically oriented, current element of strength Idℓ in free space above a half-space $z \leq 0$ having permittivity ε_1 and conductivity σ_1, Sommerfeld's formula for the Hertz potential, $\vec{\Pi}_v$, is

$$\vec{\Pi}_v(\vec{r}) = \frac{j\omega\mu_o}{4\pi} I(\vec{r}')d\ell(g_d + g_i - g_s)\,\hat{z}\,, \tag{16}$$

where

$$g_d = \exp(-jkR)/R\,,$$

$$g_i = \exp(-jkR')/R',$$

$$g_s = 2\int_0^\infty J_o(\lambda\rho'')e^{-\mu(z+z')}\,\frac{\mu_E}{\varepsilon_E\,\mu+\mu_E}\,\frac{\lambda}{\mu}\,d\lambda\,,$$

$$\vec{r} = x\hat{x} + y\hat{y} + z\hat{z}\,,$$

$$\vec{r}' = x'\hat{x} + y'\hat{y} + z'\hat{z}\,,$$

$$\rho'' = \left[(x-x')^2 + (y-y')^2\right]^{1/2},$$

$$R = |\vec{r}-\vec{r}'| = \left[\rho''^2 + (z-z')^2\right]^{1/2},$$

$$R' = \left[\rho''^2 + (z+z')^2\right]^{1/2},$$

$$\mu^2 = \lambda^2 - k^2\,,$$

$$\mu_E^2 = \lambda^2 - k_E^2\,,$$

$$k^2 = \omega^2\mu_o\varepsilon_o\,,$$

$$k_E^2 = \varepsilon_E k^2 = \frac{\varepsilon_1}{\varepsilon_o}\left(1 - \frac{j\sigma_1}{\omega\varepsilon_1}\right)k^2,$$

and J_o is the Bessel function of order 0. The electric and magnetic fields of the vertical current element are then

$$\vec{E}_v(\vec{r}) = k^2\,\vec{\Pi}_v\,(\vec{r}) + \nabla\nabla\cdot\vec{\Pi}_v(\vec{r})\,,$$

$$\vec{H}_v(\vec{r}) = \frac{jk^2}{\mu_o\omega}\,\nabla\times\vec{\Pi}_v(\vec{r}).$$

The fields of a horizontal current element are given by similar expressions which, for brevity, are omitted here but can be found in reference 13. The horizontal current produces components of the Hertz potential both parallel to the current element and in the z direction, and involves both J_o and its derivative. The Green's function for an arbitrarily oriented current is a combination of the expressions for the vertical and horizontal components. In general, however, the integral over λ for Π_v and similar integrals for a

horizontal current can not be evaluated in closed form but require numerical quadrature. Hence, integral equations derived from these expressions involve a double integration over λ and over the conducting surface. Numerical evaluation of these integrals can be very time consuming. In view of these difficulties, approximations of Sommerfeld's formulas that are easily evaluated and maintain reasonable accuracy are desirable.

One approximation for the Sommerfeld integrals employs asymptotic expansions that are valid over various ranges of the parameter values. This particular method makes use of the method of stationary phase and double saddle-point integration. Use of this approach produces closed-form expressions for the fields of an elementary source. Such expressions are useful over various ranges of observation-point location relative to the source.

A comprehensive survey of this general methodology is given by Banos (ref. 16), and the numerical accuracy of these approximations is examined by Siegel (ref. 17). Siegel's work is especially useful in that he is able to establish ranges of observation distance for which the various expressions are valid, but, unfortunately it also shows that gaps generally exist over which the approximations do not provide acceptable accuracy. This is true in particular for observation points located close to the source. Hence, the approximation is not suitable for use in integral equations, which require close proximity of observation and source points.

Other more physically based approximations have also been investigated. The reader is referred to the work by Feynberg (ref. 18), where a surface integration over the interface induced sources is discussed, with many other aspects of the problem, and the conference proceedings edited by Wait (ref. 19). The latter provides a number of interesting treatments, including one based on the compensation theorem (ref. 20) and a comparison of several formulations for antenna impedance (ref. 21).

The approximation used in NEC is primarily physically based. It is noted that in Sommerfeld's formula for Π_v, the term g_d is the direct contribution of the source and g_i is the contribution of the image of the source in a perfectly conducting ground plane. The term g_s represents the effect of an imperfectly conducting ground. For a perfectly conducting ground ($\sigma_1 \to \infty$), g_s goes to zero while for free space ($\varepsilon_1 = \varepsilon_o$, $\sigma_1 = 0$), g_s can be evaluated in closed form and exactly cancels g_i. The same observations also hold for

the horizontal current element. Hence, for a perfectly conducting ground, Sommerfeld's formulas reduce to the simple image principle.

A Green's function for a perfectly conducting ground is then the sum of the free-space Green's function of the source current element and the negative of the free-space Green's function of the mirror image of the source in the ground plane; the negative sign resulting from the change in the sign of charge on the image. If $\overline{\overline{G}}(\vec{r},\vec{r}')$ is the free-space Green's dyad for the electric field at $\vec{r}$ due to a source current at $\vec{r}'$, with $\overline{\overline{G}}$ defined in equation (1), the electric field Green's dyad, when the plane defined by $z = 0$ is perfectly conducting, is

$$\overline{\overline{G}}_{pg}(\vec{r},\vec{r}') = \overline{\overline{G}}(\vec{r},\vec{r}') + \overline{\overline{G}}_I(\vec{r},\vec{r}'), \tag{17}$$

$$(\vec{r} \cdot \hat{z}) > 0 \ , \ (\vec{r}' \ \hat{z}) > 0,$$

where

$$\overline{\overline{G}}_I(\vec{r},\vec{r}') = - \overline{\overline{I}}_r \cdot \overline{\overline{G}}(\vec{r}, \overline{\overline{I}}_r \cdot r'), \tag{18}$$

$$\overline{\overline{I}}_r = \hat{x}\hat{x} + \hat{y}\hat{y} - \hat{z}\hat{z} \ . \tag{19}$$

$\overline{\overline{I}}_r$ is a dyad that produces a reflection in the $z = 0$ plane when used in a dot product. The electric field due to current J_s on a conducting surface S above a perfect ground is then

$$\vec{E}_{pg}(\vec{r}) = \int_S \vec{J}_s(\vec{r}') \cdot \overline{\overline{G}}_{pg}(\vec{r},\vec{r}') \, dA' \ .$$

Likewise for the magnetic field, with free-space Green's dyad,

$$\overline{\overline{\Gamma}}(\vec{r},\vec{r}') = \overline{\overline{I}} \times \nabla' g(\vec{r},\vec{r}') \ , \tag{20}$$

the Green's dyad over a perfect ground is

$$\overline{\overline{\Gamma}}_{pg}(\vec{r},\vec{r}') = \overline{\overline{\Gamma}}(\vec{r},\vec{r}') + \overline{\overline{\Gamma}}_I(\vec{r},\vec{r}') \ , \tag{21}$$

$$\overline{\overline{\Gamma}}_I(\vec{r},\vec{r}') = - \overline{\overline{I}}_r \cdot \overline{\overline{\Gamma}}(\vec{r},\overline{\overline{I}}_r \cdot \vec{r}') \ , \tag{22}$$

and

$$\vec{H}_{pg}(\vec{r}) = \int_S \vec{J}_s(\vec{r}) \cdot \overline{\overline{\Gamma}}_{pg}(\vec{r},\vec{r}') \, dA' \ .$$

These modified Green's functions and their specialized forms for thin wires are easily incorporated into the integral equations (13), (14), and (15). In practice the integrals in these equations are simply extended over the structure image with only a doubling of the integration time.

The advantage of extending the ray-optics approach to the finitely conducting half-space is immediately evident. If a specularly reflected ray can be used in this case as well to account for the entire ground-reflected contribution (g_i and g_s terms) to the field, then it may be possible to circumvent the numerical difficulties of the Sommerfeld integral. Two problems arise in accomplishing this: one is the determination of the appropriate reflection coefficient for the half-space, and the other is specifying the specular ray contribution itself. These problems both occur because the fields involved are nonplane-waves and the observation point can, in general, lie in the near-field of the source where the higher order terms may be of importance.

Some insight may be gained by viewing the interface as a surface distribution of induced sources, as discussed by Feynberg (ref. 18). The ground-reflected contribution to the total field produced by a given infinitesimal source is then obtained from a surface integration over these induced sources. Practically speaking, this surface integration can be truncated to include a region of only limited extent. When the principle of stationary phase is applied, this truncated region (or essential region as denoted by Feynberg) can be shown to be generally elliptical and centered in some sense about the specular-reflection point. If the area of this essential region is allowed in the limit to shrink to zero centered on the specular point, only the specular ray itself will be obtained. Thus, a ray-optics approach based on a specular ray essentially amounts to collapsing the entire interface-induced-source distribution to a single point from which the ground-reflected field at a particular observation point to a given infinitesimal source appears to originate. This is equivalent to the use of an image source to account for the reflected field.

The finite ground conductivity consequently enters only as a modification of the image fields. For a plane-wave incident on a ground plane, the reflected field is related to the incident field by reflection coefficients derived by Fresnel (ref. 22), which are simple functions of the ground parameters and the angle of incidence of the wave. Studies have shown that the specular approximation and Fresnel reflection coefficients can be used for the near-field interaction over ground with good accuracy except between points very close to the ground (refs. 14 and 15). With this approximation, which is used in NEC, an imperfect ground is included in the integral equations with no more difficulty than is caused by a perfectly conducting ground, basically, a doubling of the integration region.

The Fresnel reflection coefficients are different for a wave polarized with electric field in or normal to the plane of incidence, which is the plane containing the normal to the ground and the vector in the direction of propagation of the incident wave. The two cases are illustrated in figure 1, where the wave with E in the plane of incidence is termed vertically polarized and with E normal to the plane of incidence as horizontally polarized. The Fresnel reflection coefficient for vertically polarized waves is

$$R_V = \frac{\cos\Theta - Z_R\sqrt{1 - Z_R^2 \sin^2\Theta}}{\cos\Theta + Z_R\sqrt{1 - Z_R^2 \sin^2\Theta}}, \tag{23}$$

where

$$\cos\Theta = -\hat{k} \cdot \hat{z},$$

$$Z_R = \left(\frac{\varepsilon_1}{\varepsilon_o} - j\frac{\sigma_1}{\omega\varepsilon_o}\right)^{-1/2}.$$

The reflected fields are then

$$\vec{E}_R^V = -R_V\left(\overline{\overline{I}}_R \cdot \vec{E}^V\right),$$

$$\vec{H}_R^V = R_V \vec{H}^V.$$

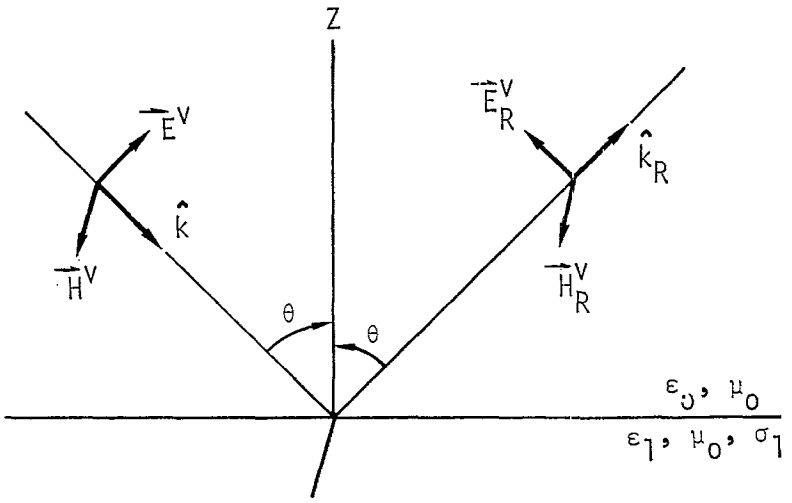

Reflection of Vertically Polarized Wave

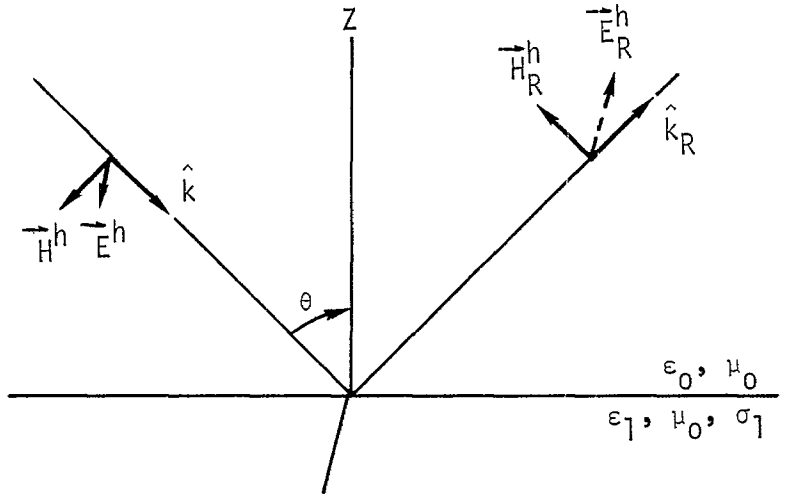

Reflection of Horizontally Polarized Wave

Figure 1. Plane-Wave Reflection at an Interface.

For horizontally polarized waves, the reflection coefficient is

$$R_H = \frac{-\left(Z_R \cos\Theta - \sqrt{1 - Z_R^2 \sin^2\Theta}\right)}{Z_R \cos\Theta + \sqrt{1 - Z_R^2 \sin^2\Theta}} , \tag{24}$$

and

$$\vec{E}_R^h = - R_H \vec{E}^h ,$$

$$\vec{H}_R^h = R_H\left(\overline{\overline{I}}_R \cdot \vec{H}^h\right) .$$

An arbitrarily polarized incident plane wave must be resolved into horizontal and vertical components to determine the reflected field. Thus, if $\hat{p}$ is the unit vector normal to the plane of incidence, the reflected field due to an incident field $\vec{E}$ is

$$\vec{E}_R = R_H(\vec{E}_I \cdot \hat{p})\hat{p} + R_V\left[\vec{E}_I - (\vec{E}_I \cdot \hat{p})\hat{p}\right]$$

$$= R_V \vec{E}_I + (R_H - R_V)(\vec{E}_I \cdot \hat{p})\hat{p} , \tag{25}$$

where $\vec{E}_I$ is the incident field reflected in a perfectly conducting ground, or the field due to the image of the source. Use of the image field in equation (25) accounts for the changes in sign and vector direction of the incident field that were shown explicitly for the vertically and horizontally polarized cases. For the magnetic field,

$$\vec{H}_R = R_H\vec{H}_I + (R_V - R_H)(\vec{H}_I \cdot \hat{p})\hat{p} , \tag{26}$$

with $\vec{H}_I$ the field of the image of the source.

Applying the Fresnel reflection coefficients to the near fields, the electric field at $\vec{r}$ due to the image of a current element at $\vec{r}'$ can be written

$$\overline{\overline{G}}_R(\vec{r},\vec{r}') = R_V\overline{\overline{G}}_I(\vec{r},\vec{r}') +$$

$$(R_H - R_V)\left[\overline{\overline{G}}_I(\vec{r},\vec{r}') \cdot \hat{p}\right]\hat{p} , \tag{27}$$

where

$$\hat{p} = \vec{p}/|\vec{p}| \ ,$$

$$\vec{p} = (\vec{r} - \vec{r}') \times \hat{z} \ ,$$

and $\overline{\overline{G}}_I$ is the Green's function for the image of the source in a perfect ground as defined in equation (18). For magnetic field, the Green's dyad for the modified image is

$$\overline{\overline{\Gamma}}_R(\vec{r},\vec{r}') = R_H \overline{\overline{\Gamma}}_I(\vec{r},\vec{r}') + (R_V - R_H)\left[\overline{\overline{\Gamma}}_I(\vec{r},\vec{r}') \cdot \hat{p}\right]\hat{p} \ . \tag{28}$$

The Green's functions for electric and magnetic fields over an imperfectly conducting ground, resulting from the reflection coefficient approximation are then

$$\overline{\overline{G}}_g(\vec{r},\vec{r}') = \overline{\overline{G}}(\vec{r},\vec{r}') + \overline{\overline{G}}_R(\vec{r},\vec{r}') \ , \tag{29}$$

$$\overline{\overline{\Gamma}}_g(\vec{r},\vec{r}') = \overline{\overline{\Gamma}}(\vec{r},\vec{r}') + \overline{\overline{\Gamma}}_R(\vec{r},\vec{r}') \ , \tag{30}$$

and the electric and magnetic fields above an imperfect ground are

$$\vec{E}_g(\vec{r}) = \int_S \vec{J}_s(\vec{r}') \cdot \overline{\overline{G}}_g(\vec{r},\vec{r}') \, dA' \ ,$$

$$\vec{H}_g(\vec{r}) = \int_S \vec{J}_s(\vec{r}') \cdot \overline{\overline{\Gamma}}_g(\vec{r},\vec{r}') \, dA' \ .$$

Use of the Green's function's $\overline{\overline{G}}_g$ and $\overline{\overline{\Gamma}}_g$ results in a straightforward extension of the EFIE and MFIE for structures over an imperfect ground. Yet, as will be demonstrated in section V by comparison with results of the Sommerfeld formulas, it provides surprisingly good results over grounds with widely varying electrical parameters. Since the method is based on a surface reflection coefficient at the specular point, it is readily adapted to a horizontally stratified half-space and to a half-space with slowly varying properties along the interface.

It has also been suggested that the reflection coefficient approximation can be used to approximate the effect of a radial-wire ground screen under

an antenna by using an approximate surface impedance for the ground screen (ref. 23). The ground-screen wires could be modeled explicitly in the NEC code. This would also be approximate, however, since the wires would have to be displaced slightly above the ground surface, in which case the reflection coefficient approximation breaks down. Explicit modeling would also greatly increase the number of unknowns in the solution. Wait (ref. 24) approximated the surface impedance of the radial-wire ground screen on an imperfectly conducting ground as the parallel combination of the surface impedance, ζ_1, of the ground plane

$$\zeta_1 = \left(\frac{j\mu_o \omega}{\sigma_1 + j\varepsilon_1 \omega} \right)^{1/2} ,$$

and an approximate surface impedance Z_g of the ground screen

$$Z_g(\rho) = \frac{j\mu_o \omega \rho}{N} \ln\left(\frac{\rho}{NC_o} \right) ,$$

which is the impedance of a parallel wire grid having the wire spacing that the radial wires have at a distance ρ from the center. N is the number of radial wires in the screen, and C_o is the radius of the wires. The surface impedance of the ground screen on an imperfect ground is then

$$\zeta_e = \frac{\zeta_1 Z_g}{\zeta_1 + Z_g} .$$

From the definition of surface impedance,

$$E_{tangential} = \zeta_e H_{tangential}$$

at the surface and using the fact that E and H in the incident wave are related by η the free-space impedance, reflection coefficients can easily be derived. They are

$$R_H = \frac{\eta - \zeta_e \cos \Theta}{\eta + \zeta_e \cos \Theta} ,$$

and

$$R_V = \frac{\eta \cos \Theta - \zeta_e}{\eta \cos \Theta + \zeta_e} .$$

This is the form the Fresnel reflection coefficients take when the index of refraction is large compared to unity, as verified when $|Z_R|^2 << 1$ in the coefficients previously presented. This condition is satisfied in most realistic problems; furthermore, the surface-impedance boundary condition is a valid approximation only when the refractive index of the ground is large compared to unity. Therefore, the surface impedance derived by Wait has been used in conjunction with the reflection coefficient method previously discussed to provide an approximate model of a radial-wire ground screen in NEC. As a result of the reflection coefficient method, only the properties of the ground directly under a vertical antenna will affect its current distribution. At the origin of the radial-wire ground screen, the impedance is zero (Z_g is not allowed to be negative) so the impedance and current distribution of a vertical antenna at the origin will be the same as over a perfect conductor. The far fields, however, will demonstrate the effect of the screen as the specular point moves away from the origin. For antennas other than the vertical antenna, it should be pointed out that the inherent polarization sensitivity of the screen (i.e., E parallel or perpendicular to the ground wires) has not been considered in this approximation.

Section III
Numerical Solution

The integral equations (13), (14), and (15) are solved numerically in NEC by a form of the method of moments. An excellent general introduction to the method of moments can be found in R. F. Harrington's book, Field Computation by Moment Methods (ref. 25). A brief outline of the method follows.

The method of moments applies to a general linear-operator equation,

$$Lf = e, \tag{31}$$

where f is an unknown response, e is a known excitation, and L is a linear operator (an integral operator in the present case). The unknown function f may be expanded in a sum of basis functions, f_j, as

$$f = \sum_{j=1}^{N} \alpha_j f_j . \tag{32}$$

A set of equations for the coefficients α_j are then obtained by taking the inner product of equation (31) with a set of weighting functions $\{w_i\}$,

$$\langle w_i, Lf \rangle = \langle w_i, e \rangle \qquad i = 1, \ldots N . \tag{33}$$

Due to the linearity of L equation (32) substituted for f yields,

$$\sum_{j=1}^{N} \alpha_j \langle w_i, Lf_j \rangle = \langle w_i, e \rangle , \qquad i = 1, \ldots N .$$

This equation can be written in matrix notation as

$$[G]\,[A] = [E] , \tag{34}$$

where

$$G_{ij} = \langle w_i, Lf_j \rangle ,$$

$$A_j = \alpha_j ,$$

$$E_i = \langle w_i, e \rangle .$$

The solution is then

$$[A] = [G]^{-1} [E] .$$

For the solution of equations (13), (14), and (15), the inner product is defined as

$$\langle f, g \rangle = \int_S f(\vec{r}) g(\vec{r}) dA ,$$

where the integration is over the structure surface. Various choices are possible for the weighting functions $\{w_i\}$ and basis functions $\{f_j\}$. When $w_i = f_i$, the procedure is known as Galerkin's method. In NEC the basis and weight functions are different, w_i being chosen as a set of delta functions

$$w_i(\vec{r}) = \delta(\vec{r} - \vec{r}_i) ,$$

with $\{\vec{r}_i\}$ a set of points on the conducting surface. The result is a point sampling of the integral equations known as the collocation method of solution. Wires are divided into short straight segments with a sample point at the center of each segment while surfaces are approximated by a set of flat patches or facets with a sample point at the center of each patch.

The choice of basis functions is very important for an efficient and accurate solution. In NEC the support of f_i is restricted to a localized subsection of the surface near $\vec{r}_i$. This choice simplifies the evaluation of the inner-product integral and ensures that the matrix G will be well conditioned. For finite N, the sum of f_j cannot exactly equal a general current distribution so the functions f_i should be chosen as close as possible to the actual current distribution. Because of the nature of the integral-equation kernels, the choice of basis function is much more critical on wires than on surfaces. The functions used in NEC are explained in the following sections.

1. CURRENT EXPANSION ON WIRES

The current on each wire segment in NEC is represented by three terms — a constant, a sine, and a cosine — with the sinusoidal terms having the free space wavelength. This expansion has been shown to provide rapid solution convergence (ref. 26 and 27) and has the added advantage that the fields of the sinusoidal currents are easily evaluated in closed form. The amplitudes of

these terms are related such that their sum satisfies physical conditions on the local behavior of current and charge at the segment ends. This differs from AMP where the current was extrapolated to the centers of the adjacent segments, resulting in discontinuities in current and charge at the segment ends. Matching at the segment ends improves the solution accuracy, especially at the multiple-wire junctions of unequal length segments where AMP extrapolated to an average length segment, often with inaccurate results.

The total current on segment number j in NEC has the form

$$I_j(s) = A_j + B_j \sin k(s-s_j) + C_j \cos k(s-s_j) \ , \qquad (35)$$

$$|s-s_j| < \Delta_j/2 \ ,$$

where s_j is the value of s at the center of segment j and Δ_j is the length of segment j. Of the three unknown constants A_j, B_j, and C_j, two are eliminated by local conditions on the current leaving one constant, related to the current amplitude, to be determined by the matrix equation. The local conditions are applied to the current and to the linear charge density, q, which is related to the current by the equation of continuity

$$\frac{\partial I}{\partial s} = - j\omega q \ . \qquad (36)$$

At a junction of two segments with uniform radius, the obvious conditions are that the current and charge are continuous at the junction. At a junction of two or more segments with unequal radii, the continuity of current is generalized to Kirchoff's current law that the sum of currents into the junction is zero. The total charge in the vicinity of the junction is assumed to distribute itself on individual wires according to the wire radii, neglecting local coupling effects. T. T. Wu and R. W. P. King (ref. 28) have derived a condition that the linear charge density on a wire at a junction, and hence $\partial I/\partial s$, is determined by

$$\left.\frac{\partial I(s)}{\partial s}\right|_{s \text{ at junction}} = \frac{Q}{\ell n\left(\frac{2}{ka}\right) - \gamma} \ , \qquad (37)$$

where a = wire radius,

$$k = 2\pi/\lambda \ ,$$

$\gamma = 0.5772$ (Euler's constant).

Q is related to the total charge in the vicinity of the junction and is constant for all wires at the junction.

At a free wire end, the current may be assumed to go to zero. On a wire of finite radius, however, the current can flow onto the end cap and hence be nonzero at the wire end. In one study of this effect, a condition relating the current at the wire end to the current derivative was derived (ref. 29). For a wire of radius a, this condition is

$$I(s)\Big|_{s \text{ at end}} = \frac{-(\hat{s}\cdot\hat{n}_c)}{k} \frac{J_1(ka)}{J_o(ka)} \frac{\partial I(s)}{\partial s}\Big|_{s \text{ at end}},$$

where J_o and J_1 are Bessel functions of order 0 and 1. The unit vector $\hat{n}_c$ is normal to the end cap. Hence, $\hat{s} \cdot \hat{n}_c$ is +1 if the reference direction, $\hat{s}$, is toward the end, and -1 is $\hat{s}$ is away from the end.

Thus, for each segment two equations are obtained from the two ends:

$$I_j(s_j \pm \Delta_j/2) = \frac{\pm 1}{k} \frac{J_1(ka_j)}{J_o(ka_j)} \frac{\partial I_j(s)}{\partial s}\Big|_{s = s_j \pm \Delta_j/2} \tag{38}$$

at free ends, and

$$\frac{\partial I_j(s)}{\partial s}\Big|_{s = s_j \pm \Delta_j/2} = \frac{Q_j^{\pm}}{\ell n\left(\frac{2}{ka_j}\right) - \gamma} \tag{39}$$

at junctions. Two additional unknowns Q_j^- and Q_j^+ are associated with the junctions but can be eliminated by Kirchoff's current equation at each junction. The boundary-condition equations provide the additional equation-per-segment to completely determine the current function of equation (35) for every segment.

To apply these conditions, the current is expanded in a sum of basis functions chosen so that they satisfy the local conditions on current and charge in any linear combination. A typical set of basis functions and their sum on a four segment wire are shown in figure 2. For a general segment i in figure 3, the i^{th} basis function has a peak on segment i and extends onto

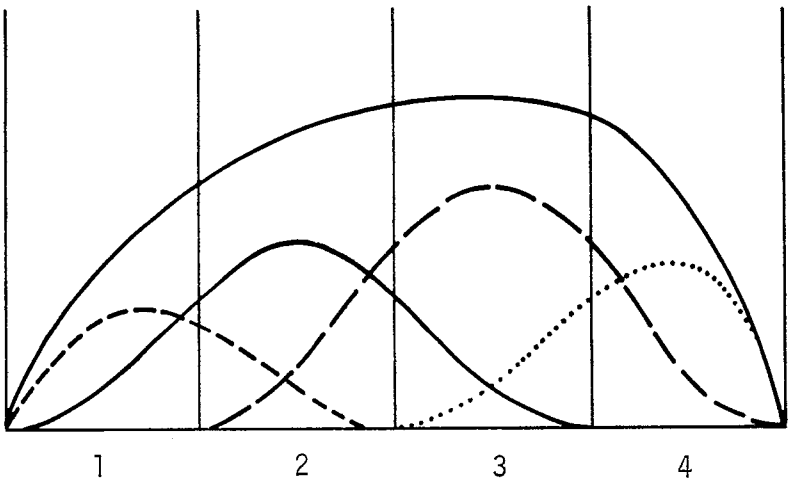

Figure 2. Current Basis Functions and Sum on a Four Segment Wire.

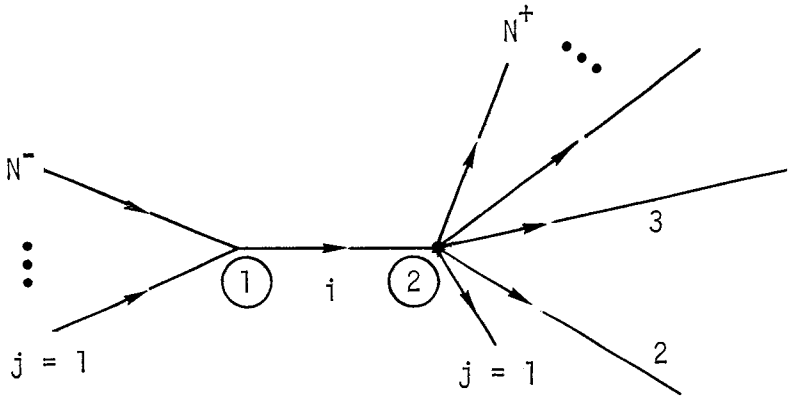

Figure 3. Segments Covered by the i^{th} Basis Function.

every segment connected to i, going to zero with zero derivative at the outer ends of the connected segments.

The general definition of the i^{th} basis function is given below. For the junction and end conditions described above, the following definitions apply for the factors in the segment end conditions:

$$a_i^- = a_i^+ = \left[\ell n \left(\frac{2}{ka_i} \right) - \gamma \right]^{-1} , \tag{40}$$

and

$$X_i = J_1(ka_i)/J_o(ka_i) .$$

The condition of zero current at a free end may be obtained by setting x_i to zero.

The portion of the i^{th} basis function on segment i is then

$$f_i^o(s) = A_i^o + B_i^o \sin k(s - s_i) + C_i^o \cos k(s - s_i) \qquad (41)$$

$$|s - s_i| < \Delta_i/2 \ .$$

If $N^- \neq 0$ and $N^+ \neq 0$, end conditions are

$$\frac{\partial}{\partial s} f_i^o(s) \Big|_{s = s_i - \Delta_i/2} = a_i^- Q_i^- \ , \qquad (42)$$

$$\frac{\partial}{\partial s} f_i^o(s) \Big|_{s = s_i + \Delta_i/2} = a_i^+ Q_i^+ \ . \qquad (43)$$

If $N^- = 0$ and $N^+ \neq 0$, end conditions are

$$f_i^o(s_i - \Delta_i/2) = \frac{1}{k} X_i \frac{\partial}{\partial s} f_i^o(s) \Big|_{s = s_i - \Delta_i/2} \qquad (44)$$

$$\frac{\partial}{\partial s} f_i^o(s) \Big|_{s = s_i + \Delta_i/2} = a_i^+ Q_i^+ \ . \qquad (45)$$

If $N^- \neq 0$ and $N^+ = 0$, end conditions are

$$\frac{\partial}{\partial s} f_i^o(s) \Big|_{s = s_i - \Delta_i/2} = a_i^- Q_i^- \ , \qquad (46)$$

$$f_i^o(s_i + \Delta_i/2) = \frac{-1}{k} X_i \frac{\partial}{\partial s} f_i^o(s) \Big|_{s = s_i + \Delta_i/2} \ . \qquad (47)$$

Over segments connected to end 1 of segment i, the i^{th} basis function is

$$f_j^-(s) = A_j^- + B_j^- \sin k(s - s_j) + C_j^- \cos k(s - s_j) \qquad (48)$$

$$|s - s_j| < \Delta_j/2 \quad j = 1, \ \ldots \ , N^- \ .$$

End conditions are

$$f_j^-(s_j - \Delta_j/2) = 0 \ , \tag{49}$$

$$\frac{\partial}{\partial s} f_j^-(s) \Big|_{s = s_j - \Delta_j/2} = 0 \ , \tag{50}$$

$$\frac{\partial}{\partial s} f_j^-(s) \Big|_{s = s_j + \Delta_j/2} = a_j^+ Q_i^- \ . \tag{51}$$

Over segments connected to end 2 of segment i, the i^{th} basis function is

$$f_j^+(s) = A_j^+ + B_j^+ \sin k(s - s_j) + C_j^+ \cos k(s - s_j) \tag{52}$$

$$|s - s_j| < \Delta_j/2 \quad j = 1, \ \ldots \ , N^+ \ .$$

End conditions are

$$\frac{\partial}{\partial s} f_j^+(s) \Big|_{s = s_j - \Delta_j/2} = a_j^- Q_i^+ \ , \tag{53}$$

$$f_j^+(s_j + \Delta_j/2) = 0 \ , \tag{54}$$

$$\frac{\partial}{\partial s} f_j^+(s) \Big|_{s = s_j + \Delta_j/2} = 0 \ . \tag{55}$$

Equations (41), (48), and (52), defining the complete basis function, involve $3(N^- + N^+ + 1)$ unknown constants. Of these, $3(N^- + N^+) + 2$ unknowns are eliminated by the end conditions in terms of Q_i^- and Q_i^+ which can then be determined from the two Kirchoff's current equations:

$$\sum_{j=1}^{N^-} f_j^-(s_j + \Delta_j/2) = f_i^o(s_i - \Delta_i/2) \ , \text{ and} \tag{56}$$

$$\sum_{j=1}^{N^+} f_j^+(s_j - \Delta_j/2) = f_i^o(s_i + \Delta_i/2) \ . \tag{57}$$

The complete basis function is then defined in terms of one unknown constant. In this case A_i^o was set to -1 since the function amplitude is arbitrary, being determined by the boundary condition equations. The final result is given below:

$$A_j^- = \frac{a_j^+ Q_i^-}{\sin k \Delta_j} , \tag{58}$$

$$B_j^- = \frac{a_j^+ Q_i^-}{2 \cos k \Delta_j/2} , \tag{59}$$

$$C_j^- = \frac{- a_j^+ Q_i^-}{2 \sin k \Delta_j/2} , \tag{60}$$

$$A_j^+ = \frac{- a_j^- Q_i^+}{\sin k \Delta_j} , \tag{61}$$

$$B_j^+ = \frac{a_j^- Q_i^+}{2 \cos k \Delta_j/2} , \tag{62}$$

$$C_j^+ = \frac{a_j^- Q_i^+}{2 \sin k \Delta_j/2} . \tag{63}$$

For $N^- \neq 0$ and $N^+ \neq 0$,

$$A_i^o = - 1 , \tag{64}$$

$$B_i^o = \left(a_i^- Q_i^- + a_i^+ Q_i^+\right) \frac{\sin k \Delta_i/2}{\sin k \Delta_i} , \tag{65}$$

$$C_i^o = \left(a_i^- Q_i^- - a_i^+ Q_i^+\right) \frac{\cos k \Delta_i/2}{\sin k \Delta_i} , \tag{66}$$

$$Q_i^- = \frac{a_i^+(1 - \cos k\,\Delta_i) - P_i^+ \sin k\,\Delta_i}{\left(P_i^- P_i^+ + a_i^- a_i^+\right)\sin k\,\Delta_i + \left(P_i^- a_i^+ - P_i^+ a_i^-\right)\cos k\,\Delta_i}\,, \tag{67}$$

$$Q_i^+ = \frac{a_i^-(\cos k\,\Delta_i - 1) - P_i^- \sin k\,\Delta_i}{\left(P_i^- P_i^+ + a_i^- a_i^+\right)\sin k\,\Delta_i + \left(P_i^- a_i^+ - P_i^+ a_i^-\right)\cos k\,\Delta_i}\,. \tag{68}$$

For $N^- = 0$ and $N^+ \neq 0$,

$$A_i^o = -1\,, \tag{69}$$

$$B_i^o = \frac{\sin k\,\Delta_i/2}{\cos k\,\Delta_i - X_i \sin k\,\Delta_i} + a_i^+ Q_i^+ \frac{\cos k\,\Delta_i/2 - X_i \sin k\,\Delta_i/2}{\cos k\,\Delta_i - X_i \sin k\,\Delta_i}\,, \tag{70}$$

$$C_i^o = \frac{\cos k\,\Delta_i/2}{\cos k\,\Delta_i - X_i \sin k\,\Delta_i} + a_i^+ Q_i^+ \frac{\sin k\,\Delta_i/2 - X_i \cos k\,\Delta_i/2}{\cos k\,\Delta_i - X_i \sin k\,\Delta_i} \tag{71}$$

$$Q_i^+ = \frac{\cos k\,\Delta_i - 1 - X_i \sin k\,\Delta_i}{\left(a_i^+ + X_i P_i^+\right)\sin k\,\Delta_i + \left(a_i^+ X_i - P_i^+\right)\cos k\,\Delta_i} \tag{72}$$

For $N^- \neq 0$ and $N^+ = 0$,

$$A_i^o = -1\,, \tag{73}$$

$$B_i^o = \frac{-\sin k\,\Delta_i/2}{\cos k\,\Delta_i - X_i \sin k\,\Delta_i} + a_i^- Q_i^- \frac{\cos k\,\Delta_i/2 - X_i \sin k\,\Delta_i/2}{\cos k\,\Delta_i - X_i \sin k\,\Delta_i}\,, \tag{74}$$

$$C_i^o = \frac{\cos k\,\Delta_i/2}{\cos k\,\Delta_i - X_i \sin k\,\Delta_i} - a_i^- Q_i^- \frac{\sin k\,\Delta_i/2 + X_i \cos k\,\Delta_i/2}{\cos k\,\Delta_i - X_i \sin k\,\Delta_i}\,, \tag{75}$$

$$Q_i^- = \frac{1 - \cos k\,\Delta_i + X_i \sin k\,\Delta_i}{\left(a_i^- - X_i P_i^-\right)\sin k\,\Delta_i + \left(P_i^- + X_i a_i^-\right)\cos k\,\Delta_i}\,. \tag{76}$$

For all cases,

$$P_i^- = \sum_{j=1}^{N^-} \left(\frac{1 - \cos k \Delta_j}{\sin k \Delta_j} \right) a_j^+ , \tag{77}$$

$$P_i^+ = \sum_{j=1}^{N^+} \left(\frac{\cos k \Delta_j - 1}{\sin k \Delta_j} \right) a_j^- , \tag{78}$$

where the sum for P_i^- is over segments connected to end 1 of segment i, and the sum for P_i^+ is over segments connected to end 2. If $N^- = N^+ = 0$, the complete basis function is

$$f_i^o = \frac{\cos k(s - s_i)}{\cos k \Delta_i/2 - X_i \sin \Delta_i/2} - 1 . \tag{79}$$

When a segment end is connected to a ground plane or to a surface modeled with the MFIE, the end condition on both the total current and the last basis function is

$$\frac{\partial}{\partial s} I_j(s) \Big|_{s = s_j \pm \Delta_j/2} = 0 ,$$

replacing the zero current condition at a free end. This condition does not require a separate treatment, however, but is obtained by computing the last basis function as if the last segment is connected to its image segment on the other side of the surface.

It should be noted that in AMP, the basis function f_i has unit value at the center of segment i and zero value at the centers of connected segments although it does extend onto the connected segments. As a result, the amplitude of f_i is the total current at the center of segment i. This is not true in NEC so the current at the center of segment i must be computed by summing the contributions of all basis functions extending onto segment i.

2. CURRENT EXPANSION ON SURFACES

The surface current is expanded in a set of pulse functions except in the region of a wire connection, as will be described later. The pulse function expansion for N_p patches is

$$\vec{J}_s(\vec{r}) = \sum_{j=1}^{N_p} (J_{1j}\ \hat{t}_{1j} + J_{2j}\ \hat{t}_{2j})\ V_j(\vec{r}) \ , \tag{80}$$

where

$$\hat{t}_{1j} = \hat{t}_1(\vec{r}_j) \ ,$$

$$\hat{t}_{2j} = \hat{t}_2(\vec{r}_j) \ ,$$

$\vec{r}_j$ = position of the center of patch number j ,

$V_j(\vec{r})$ = 1 for $\vec{r}$ on patch j and 0 otherwise.

The constants J_{1j} and J_{2j}, representing average surface-current density over the patch, are determined by the solution of the linear system of equations derived from the integral equations. The integrals for fields, due to the pulse basis functions, are evaluated numerically in a single step so that for integration, the pulses could be reduced to delta functions at the patch centers. That this simple approximation of the current yields good accuracy is one of the advantages of the MFIE for surfaces.

A more realistic representation of the surface current is needed, however, in the region where a wire connects to the surface. The treatment used in NEC, affecting the four coplanar patches about the connection point, is quite similar to that used by Albertsen et al. (ref. 9). In the region of the wire connection, the surface current contains a singular component due to the current flowing from the wire onto the surface. The total surface current should satisfy the condition,

$$\nabla_s \cdot \vec{J}_s(x,y) = J_o(x,y) + I_o\delta(x,y) \ ,$$

where the local coordinates x and y are defined in figure 4, ∇_s denotes surface divergence, $J_o(x,y)$ is a continuous function in the region ABCD, and I_o is the current at the base of the wire flowing onto the surface. One expansion which meets this requirement is

$$\vec{J}_s(x,y) = I_o\vec{f}(x,y) + \sum_{j=1}^{4} g_j(x,y)(\vec{J}_j - I_o\ \vec{f}_j) \ , \tag{81}$$

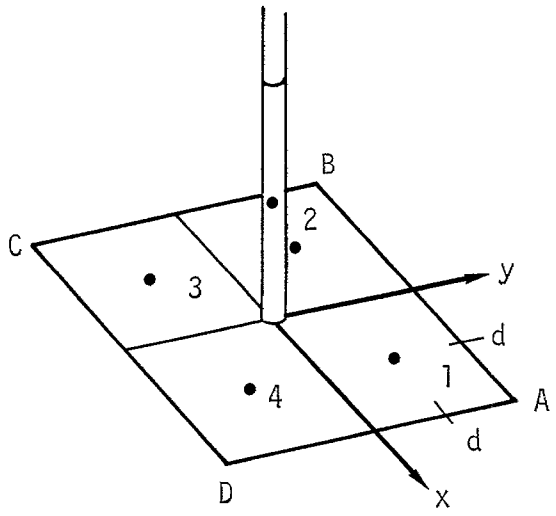

Figure 4. Detail of the Connection of a Wire to a Surface.

where

$$\vec{f}(x,y) = \frac{x\hat{x} + y\hat{y}}{2\pi(x^2 + y^2)} ,$$

$$\vec{J}_j = \vec{J}_s(x_j,y_j) ,$$

$$\vec{f}_j = \vec{f}(x_j,y_j) , \text{ and}$$

$(x_j,y_j) = (x,y)$ at the center of patch j. The interpolation functions $g_j(x,y)$ are chosen such that: $g_j(x,y)$ is differentiable on ABCD; $g_j(x_i,y_i) = \delta_{ij}$; and $\sum_{j=1}^{4} g_j(x,y) = 1$. The specific functions used in NEC are as follows:

$$g_1(x,y) = \frac{1}{4d^2}(d+x)(d+y) \qquad g_2(x,y) = \frac{1}{4d^2}(d-x)(d+y)$$

$$g_3(x,y) = \frac{1}{4d^2}(d-x)(d-y) \qquad g_4(x,y) = \frac{1}{4d^2}(d+x)(d-y)$$

Equation (81) is used when computing the electric field at the center of the connected wire segment due to the surface current on the four surrounding patches. In computing the field on any other segments or on any patches, the pulse-function form is used for all patches including those at the connection point. This saves integration time and is sufficiently accurate for the greater source to observation-point separations involved.

3. THE MATRIX EQUATION FOR CURRENT

For a structure having N_s wire segments and N_p patches, the order of the matrix in equation (34) is $N = N_s + 2N_p$. In NEC the wire segment equations occur first in the linear system so that, in terms of submatrices, the equation has the form

$$\begin{bmatrix} A & B \\ C & D \end{bmatrix} \begin{bmatrix} I_w \\ I_p \end{bmatrix} = \begin{bmatrix} E_w \\ H_p \end{bmatrix} ,$$

with equations derived from equation (14) in odd numbered rows in the lower set and equation (15) in even rows. I_w is then the column vector of segment basis function amplitudes, and I_p is the patch-current amplitudes (J_{1j}, J_{2j}, $j=1,\ldots,N_p$). The elements of E_w are the left-hand side of equation (13) evaluated at segment centers, while H_p contains, alternately, the left-hand sides of equations (14) and (15) evaluated at patch centers.

A matrix element A_{ij} in submatrix A represents the electric field at the center of segment i due to the j^{th} segment basis function, centered on segment j. A matrix element D_{ij} in submatrix D represents a tangential magnetic field component at patch k due to a surface-current pulse on patch ℓ where

$$k = \text{Int}\left[(i-1)/2\right] + 1 ,$$

$$\ell = \text{Int}\left[(j-1)/2\right] + 1 ,$$

and Int[] indicates truncation. The source pulse is in the direction $\hat{t}_1$ when j is odd, and direction $\hat{t}_2$ when j is even. When $k = \ell$ the contribution of the surface integral is zero since the vector product is zero on the flat patch surface, although a ground image may produce a contribution. However, for $k = \ell$, there is a contribution of $\pm 1/2$ from the coefficient of $\vec{J}_s(\vec{r})$ in equation (14) or (15). Matrix elements in submatrices B and C represent electric fields due to surface-current pulses and magnetic fields due to segment basis functions, respectively. These present no special problems since the source and observation points are always separated.

4. SOLUTION OF THE MATRIX EQUATION

The matrix equation,

$$[G]\,[I] = [E] , \qquad (82)$$

is solved in NEC by the Gauss-Doolittle technique (ref. 30) which is a variant of the well-known Gauss elimination method. The basic step in the Gauss-Doolittle method is factorization of the matrix G into the product of an upper triangular matrix U and a lower triangle matrix L where

$$G = [L]\ [U]\ .$$

The matrix equation is then

$$[L]\ [U]\ [I] = [E]\ , \tag{83}$$

from which the solution, I, is computed in two steps as

$$[L]\ [F] = [E]\ , \tag{84}$$

and

$$[U]\ [I] = [F]\ . \tag{85}$$

Equation (84) is first solved for F by forward substitution, and equation (85) is then solved for I by backward substitution.

The major computational effort is factoring G into L and U. This takes approximately $1/3\ N^3$ multiplication steps for a matrix of order N compared to N^3 for inversion of G by the Gauss-Jordan method. Solution of equations (84) and (85), making use of the triangular properties of L and U, takes approximately as many multiplications as would be required for multiplication of G^{-1} by the column vector E. The factored matrices L and U are saved in NEC since the solution for induced current may be repeated for a number of different excitations. This, then, requires only the repeated solution of equations (84) and (85).

Computation of the elements of the matrix G and solution of the matrix equation are the two most time-consuming steps in computing the response of a structure, often accounting for over 90% of the computation time. This may be reduced substantially by making use of symmetries of the structure, either symmetry about a plane, or symmetry under rotation.

In rotational symmetry, a structure having M sectors is unchanged when rotated by any multiple of 360/M degrees. If the equations for all segments and patches in the first sector are numbered first and followed by successive sectors in the same order, the matrix equation can be expanded in submatrices in the form

$$\begin{bmatrix} A_1 & A_2 & A_3 & \cdots & A_{M-1} & A_M \\ A_M & A_1 & A_2 & \cdots & A_{M-2} & A_{M-1} \\ A_{M-1} & A_M & A_1 & & A_{M-3} & A_{M-2} \\ \vdots & & & & \vdots & \vdots \\ A_2 & A_3 & A_4 & & A_M & A_1 \end{bmatrix} \begin{bmatrix} I_1 \\ I_2 \\ I_3 \\ \vdots \\ I_M \end{bmatrix} = \begin{bmatrix} E_1 \\ E_2 \\ E_3 \\ \vdots \\ E_M \end{bmatrix} \tag{86}$$

If there are N_c equations in each sector, E_i and I_i are N_c element column vectors of the excitations and currents in sector i. A_i is a submatrix of order N_c containing the interaction fields in sector 1 due to currents in sector i. Due to symmetry, this is the same as the fields in sector k due to currents in sector i + k, resulting in the repetition pattern shown. An immediate result is that only matrix elements in the first row of submatrices need be computed, reducing the time to fill the matrix by a factor of 1/M.

The time to solve the matrix equation can also be reduced by expanding the excitation subvectors in a discrete Fourier series as

$$E_i = \sum_{k=1}^{M} S_{ik} \mathcal{E}_k \qquad i=1,\ldots,M \ , \tag{87}$$

$$\mathcal{E}_i = \frac{1}{M} \sum_{k=1}^{M} S^*_{ik} E_k \qquad i=1,\ldots,M \ , \tag{88}$$

where

$$S_{ik} = \exp\left[j2\pi(i-1)(k-1)/M\right] \ , \tag{89}$$

$j=\sqrt{-1}$, and * indicates the conjugate of the complex number. Examining a component in the expansion,

$$E = \begin{bmatrix} S_{1k} \mathcal{E}_k \\ S_{2k} \mathcal{E}_k \\ \vdots \\ S_{Mk} \mathcal{E}_k \end{bmatrix} \ , \tag{90}$$

it is seen that the excitation differs from sector to sector only by a uniform phase shift. This excitation of a rotationally symmetric structure results in a solution having the same form as the excitation, i.e.,

$$I = \begin{bmatrix} S_{1k}\, I_k \\ S_{2k}\, I_k \\ \cdot \\ \cdot \\ \cdot \\ S_{Mk}\, I_k \end{bmatrix} . \tag{91}$$

It can be shown that this relation between solution and excitation holds for any matrix having the form of that in equation (86). Substituting these components of E and I into equation (86) yields the following matrix equation of order N_c relating I_k to E_k:

$$\left[S_{1k}\, A_1 + S_{2k}\, A_2 + \ldots + S_{Mk}\, A_M\right] \left[I_k\right] = S_{1k} \left[E_k\right] . \tag{92}$$

The solution for the total excitation is then obtained by an inverse transformation,

$$I_i = \sum_{k=1}^{M} S_{ik}\, I_k \qquad i=1, \ldots, M . \tag{93}$$

The solution procedure, then, is first to compute the M submatrices A_i and Fourier-transform these to obtain

$$A_i = \sum_{k=1}^{M} S_{ik}\, A_k \qquad i=1, \ldots, M . \tag{94}$$

The matrices A_i, of order N_c, are then each factored into upper and lower triangular matrices by the Gauss-Doolittle method. For each excitation vector, the transformed subvectors are then computed by equation (88) and the transformed current subvectors are obtained by solving the M equations,

$$[A_i]\, [I_i] = [E_i] . \tag{95}$$

The total solution is then given by equation (93).

The same procedure can be used for structures that have planes of symmetry. The Fourier transform is then replaced by even and odd excitations about each symmetry plane. All equations remain the same with the exception that the matrix S with elements S_{ij}, given by equation (89), is replaced by the following matrices:

For one plane of symmetry,

$$S = \begin{bmatrix} 1 & 1 \\ 1 & -1 \end{bmatrix};$$

For two orthogonal planes of symmetry,

$$S = \begin{bmatrix} 1 & 1 & 1 & 1 \\ 1 & -1 & 1 & -1 \\ 1 & 1 & -1 & -1 \\ 1 & -1 & -1 & 1 \end{bmatrix};$$

and for three orthogonal symmetry planes,

$$S = \begin{bmatrix} 1 & 1 & 1 & 1 & 1 & 1 & 1 & 1 \\ 1 & -1 & 1 & -1 & 1 & -1 & 1 & -1 \\ 1 & 1 & -1 & -1 & 1 & 1 & -1 & -1 \\ 1 & -1 & -1 & 1 & 1 & -1 & -1 & 1 \\ 1 & 1 & 1 & 1 & -1 & -1 & -1 & -1 \\ 1 & -1 & 1 & -1 & -1 & 1 & -1 & 1 \\ 1 & 1 & -1 & -1 & -1 & -1 & 1 & 1 \\ 1 & -1 & -1 & 1 & -1 & 1 & 1 & -1 \end{bmatrix}.$$

For either rotational or plane symmetry, the procedure requires factoring of M matrices of order N_c rather than one matrix of order MN_c. Each excitation then requires the solution of the M matrix equations. Since the time for factoring is approximately proportional to the cube of the matrix order and the time for solution is proportional to the square of the order, the symmetry results in a reduction of factor time by M^{-2} and in solution time by M^{-1}. The time to compute the transforms is generally small compared to the time for matrix operations since it is proportional to a lower power of N_c. Symmetry also reduces the number of locations required for matrix

storage by M^{-1} since only the first row of submatrices need be stored. The transformed matrices, A_i, can replace the matrices A_i as they are computed.

If part of a complete structure is symmetric but the remainder is not, advantage can still be taken of the symmetry by partitioning the matrix into symmetric and unsymmetric sections. For a matrix partitioned into submatrices as

$$\begin{bmatrix} A & B \\ C & D \end{bmatrix} \begin{bmatrix} I_1 \\ I_2 \end{bmatrix} = \begin{bmatrix} E_1 \\ E_2 \end{bmatrix} ,$$

the solution can be computed as

$$I_2 = \left[D - CA^{-1}B\right]^{-1} \left[E_2 - CA^{-1} E_1\right] ,$$

$$I_1 = A^{-1} E_1 - A^{-1} BI_2 ,$$

where multiplication of a matrix inverse by a column vector on the right can be replaced by the Gauss-Doolittle solution procedure. Then, if A represents the interaction of the symmetric section, the symmetric factoring and solution procedures can be used for products involving A^{-1}. This solution for partial symmetry is not in the standard NEC deck although the solution for complete symmetry, either rotational or plane, is implemented.

Section IV
Modeling of Antennas

Previous sections have dealt with the problem of determining the current induced on a structure by an arbitrary excitation. We now consider some specific problems in modeling antennas and scatterers, including models for a voltage source on a wire, lumped and distributed loads, nonradiating networks, and transmission lines. Calculations of some observable quantities are also covered including input impedance, radiated field, and antenna gain.

1. SOURCE MODELING

The approach used in NEC is applicable to a number of electromagnetic analysis problems. For receiving antennas and EMP studies, the excitation is the field of an incident plane wave and the desired response is the induced current at one or more points on the structure. In scattering analysis the excitation is still an incident plane wave, but the desired response is the field radiated by the induced currents. In the case of a wire transmitting antenna, however, the excitation is generally a voltage source on the wire. The antenna source problem has received a considerable amount of attention in the literature. A rather thorough exposition on the appropriate source configuration for the linear dipole antenna has been given by King (ref. 31). The delta-function source, which may be visualized as an infinitesimally thin, circumferential belt of axially directed electric field [or, alternatively, as a frill of magnetic current at the antenna feed point (ref. 32)], is convenient mathematically, but of somewhat questionable physical realizability. Since the excitation can be specified only at discrete points in NEC, a delta-function source is not feasible.

A useful source model, however, is an electric field specified at a single match point. For a voltage source of strength V on segment i, the element in the excitation vector corresponding to the applied electric field at the center of segment i is set to

$$E_i = \frac{V}{\Delta_i} \quad , \tag{96}$$

where Δ_i is the length of segment i. The direction of E_i is toward the positive end of the voltage source so that it pushes charge in the same direction as the source. The field at other match points is set to zero.

The actual effective voltage is the line integral of the applied field along the wire. This cannot be determined beforehand since the field is known only at segment centers, but can be determined after the solution for current by integrating the scattered field produced by the current. For equal length segments in the vicinity of the source this field, which must be the negative of the applied field at every point on the wire, is nearly constant over segment i and drops sharply at the segment ends. This results in an actual voltage of approximately $\Delta_i E_i$ as assumed in equation (96). When the source segment and adjacent segments are not of equal length, however, the actual voltage, obtained by integrating the scattered field, may differ from the intended value.

Ideally, this source model applies a voltage V between the ends of the source segment. Hence, the antenna input admittance could be computed as the current at the segment ends or, in an unsymmetric case, the average of the current at the two ends, divided by the applied voltage. In practice the segment is sufficiently short so that the current variation over its length is small and the current at the center can be used rather than the ends. When segment lengths in the source region are unequal, the computed input admittance may be inaccurate due to the discrepancy between the actual and assumed voltages. Use of the actual voltage, obtained by integrating the near field, will generally give an accurate admittance although it will require additional effort for computation.

An alternate source model that is less sensitive to the equality of segment lengths in the source region is based on a discontinuity in the derivative of current. This source model is similar to one used by Andreasen and Harris (ref. 33), and its use in a program similar to NEC was reported by Adams, Poggio, and Miller (ref. 34). For this model, the source region is viewed as a biconical transmission line with feed point at the source location, as illustrated in figure 5. The voltage between a point at s and the symmetric point on the other side of the line is then related to the derivative of the current by the transmission line equation,

$$V(s) = - jZ_o \frac{\partial I(ks)}{\partial (ks)} \quad , \tag{97}$$

where Z_o is the characteristic impedance of the transmission line. The characteristic impedance of a biconical transmission line of half-angle Θ is

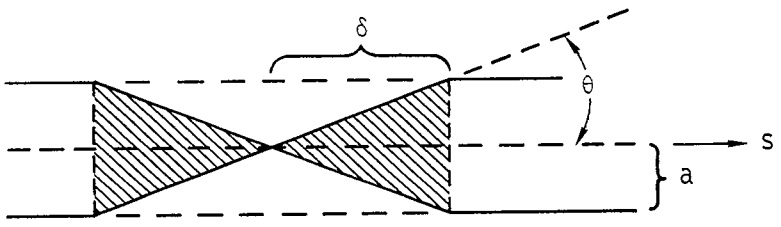

Figure 5. Biconical Transmission Line Model of Source Region.

$$Z_o = 120\ \ell n\left(\cot\frac{\Theta}{2}\right) ,$$

or for small angles,

$$Z_o \approx 120\ \ell n\left(\frac{2}{\Theta}\right) . \tag{98}$$

For a source on a wire, however, the proper choice for δ in figure 5, defining the angle Θ, is unclear. Adams et al. (ref. 34) used an average value of Z_o obtained by averaging equation (98) for δ ranging from zero to d as

$$Z_{avg} = \frac{1}{d}\int_o^d 120\ \ell n\left(\frac{2\delta}{a}\right) d\delta$$

$$= 120\left[\ell n\left(\frac{2d}{a}\right) - 1\right] ,$$

where d is set equal to the distance from the source location at the segment end to the match point at the segment center. The voltage across the line is then

$$V(s) = -\,j\ 120\left[\ell n\left(\frac{2d}{a}\right) - 1\right]\frac{\partial I(ks)}{\partial(ks)} .$$

Allowing for a current unsymmetric about the source, the voltage V_o of a source at s_o is related to a discontinuity in current derivative as

$$\lim_{\varepsilon\to o}\left[\left.\frac{\partial I(ks)}{\partial(ks)}\right|_{s = s_o + \varepsilon} - \left.\frac{\partial I(ks)}{\partial(ks)}\right|_{s = s_o - \varepsilon}\right] =$$

$$\frac{-jV_o}{60\left[\ell n\left(\frac{2d}{a}\right) - 1\right]} . \tag{99}$$

This discontinuity in current derivative is introduced into NEC by modifying the current expansion on the wire. The normal expansion for N_s wire segments is

$$I(s) = \sum_{j=1}^{N_s} \alpha_j \, f_j(s) \ ,$$

where the basis functions, f_j, are defined in section III-1 such that I(s) has continuous value and derivative along wires, and satisfies Kirchoff's law and a condition on charge density at junctions.

For a current-slope-discontinuity source at the first end of segment ℓ, the current expansion is modified to

$$I(s) = \sum_{j=1}^{N_s} \alpha_j \, f_j(s) + \beta_\ell \, f^*_\ell(s) \ , \qquad (100)$$

where f^*_ℓ is a basis function for segment ℓ, as defined in section III-1, but computed as if the first end of segment ℓ were a free end and the segment radius were zero. Hence, f^*_ℓ goes to zero with nonzero derivative at the source location.

If f^*_ℓ on segment ℓ is

$$f^*_\ell(s) = A^*_\ell + B^*_\ell \sin k(s - s_\ell) + C^*_\ell \cos k(s - s_\ell)$$

$$|s - s_\ell| < \Delta_\ell/2 \ ,$$

then

$$\frac{\partial}{\partial(ks)} f^*_\ell(s) \Big|_{s = s_\ell - \Delta_\ell/2} = B^*_\ell \cos(k\Delta_\ell/2) + C^*_\ell \sin(k\Delta_\ell/2) \ .$$

Since the sum of the normal basis functions has continuous value and derivative at $s = s_\ell - \Delta_\ell/2$, the current in equation (100) has a discontinuity in derivative of

$$\lim_{\varepsilon \to o} \left\{ \frac{\partial}{\partial(ks)} I(s) \Big|_{s=s_\ell - \Delta_\ell/2 + \varepsilon} - \frac{\partial}{\partial(ks)} I(s) \Big|_{s=s_\ell - \Delta_\ell/2 - \varepsilon} \right\} =$$

$$\beta_\ell \left\{ B^*_\ell \cos(k\Delta_\ell/2) + C^*_\ell \sin(k\Delta_\ell/2) \right\} .$$

Hence, from equation (99), a source voltage of V_o requires a value of β_ℓ in the current expansion of

$$\beta_\ell = \frac{-jV_o}{60} \left\{ \left[\ell n\left(\frac{\Delta_\ell}{a_\ell}\right) - 1 \right] \left[B_\ell^* \cos(k\Delta_\ell/2) + C_\ell^* \sin(k\Delta_\ell/2) \right] \right\}^{-1} . \tag{101}$$

The linear system for the current expansion constants, obtained by substituting equation (100) for f in equation (33), is

$$\sum_{j=1}^{N_s} \alpha_j \langle w_i, Lf_j \rangle = \langle w_i, e \rangle - \beta_\ell \langle w_i, f_\ell^* \rangle . \tag{102}$$

$$i = 1, \ldots N_s$$

In matrix notation, corresponding to equation (34),

$$[G]\,[A] = [E] + \beta_\ell\,[F] , \tag{103}$$

where F_i is the excitation for segment or patch equation number i due to the field of f_ℓ^*, and E_i is the excitation for segment or patch equation number i from other sources (if there are any). The interaction matrix G is independent of this source as it is of other sources. The solution for the expansion coefficients is then

$$[A] = [G^{-1}] \left\{ [E] + \beta_\ell\,[F] \right\} ,$$

where A supplies the coefficients α_j in equation (100) to determine the current. This method is easily extended to several sources. The modified basis function f_ℓ^* appears to introduce an asymmetry into the current, but this is not the case since the other basis function amplitudes are free to adjust accordingly.

The current-slope-discontinuity source results in an effective applied field that is much more localized in the source region than that of the constant-field source defined by equation (96). The difference is shown in near-field plots for the two source models in figure 6, taken from Adams

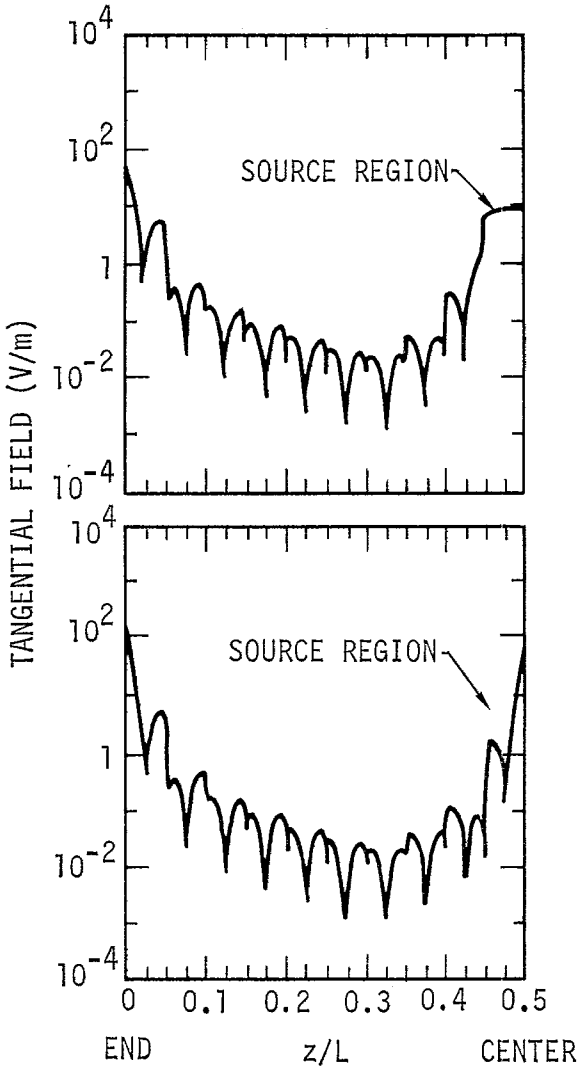

Figure 6. Field Plots for a Linear Dipole, Ω=15.

et al. (ref. 34). The near fields are for a half wavelength dipole antenna with $\Omega = 15$ [$\Omega = 2\ell n(L/a)$, L = length, a = radius] and with 10 segments on half of the antenna covered by the plots. The constant-field source is seen to result in a nearly rectangular field distribution in the source region while the field of the slope-discontinuity source approaches a delta function. The integrals of these two source-field distributions yield approximately the same voltages, however.

With the slope-discontinuity-source model, the input admittance is the ratio of the current at the segment end, where the source is located, to the source voltage. Adams et al. also present results showing the effect on admittance of varying the source-segment length relative to the lengths of adjacent segments, showing that the slope-discontinuity source is much less sensitive to segment length than is the constant-field source. The two segments on opposite sides of the source must have equal lengths and radii, however. For very short, segment lengths, the slope-discontinuity model may break down although, as with the constant-field source, the correct admittance can be obtained by integrating the near field to obtain the source voltage.

2. NONRADIATING NETWORKS

Antennas often include transmission lines, lumped circuit networks, or a combination of both connecting between different parts or elements. When the currents on transmission lines or at network ports are balanced, the resulting fields cancel and can often be neglected, greatly simplifying the

modeling problem. The solution procedure used in NEC is to compute a driving-point-interaction matrix from the complete segment-interaction matrix. The driving-point matrix relates the voltages and currents at network connection points as required by the electromagnetic interactions. The driving-point-interaction equations are then solved together with the network or transmission line equations to obtain the induced currents and voltages. In this way the larger segment-interaction matrix is not changed by addition or modification of networks or transmission lines.

The solution described below assumes an electromagnetic interaction matrix equation of the form,

$$[G]\,[I] = -\,[E]\ , \tag{104}$$

where E_i is the exciting electric field on wire segment i and I_i is the current at the center of segment i. In NEC the interaction equation has the form,

$$[G]\,[A] = -\,[E]\ ,$$

where A_i is the amplitude of the i^{th} basis function f_i in the current expansion,

$$I(s) = \sum_{i=1}^{N_s} A_i\, f_i(s)\ .$$

The same solution technique can be used, however, by computing I from A whenever I is needed. This must be done in computing the elements of the inverse of G, G^{-1}_{ij}, which below represent the current on segment i due to a unit field on segment j.

A model consisting of N_s segments will be assumed with a general M-port network connected to segments 1 through M. The network is described by the admittance equations,

$$\sum_{j=1}^{M} Y_{ij}\, V_j = I_i^t \qquad i=1,\ \ldots,\ M\ , \tag{105}$$

where V_i and I_i^t are the voltage and current at port i, with reference directions as shown in figure 7.

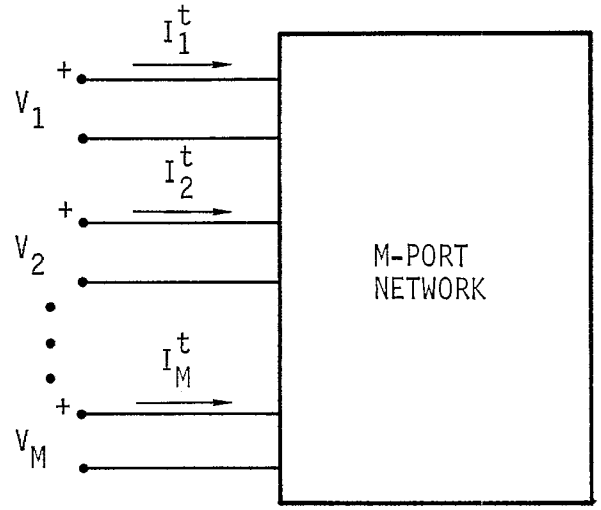

Figure 7. Voltage and Current Reference Directions at Network Ports.

The connection of a network port to a segment is illustrated in figure 8. The segment is broken, and the port is connected so that

$$I_i^t = - I_i \ , \tag{106}$$

where I_i is the segment current. Figure 9 shows a voltage source of strength V_i connected across the network port at segment i. In this case,

$$I_i^t = I_i^g - I_i \ . \tag{107}$$

In either case, the port voltage may be related to the applied field on the segment by the constant-field voltage source model of equation (96).

We will assume that segments 1 through M_1 are connected to network ports without voltage sources, and segments $M_1 + 1$ through M are connected to network ports with voltage sources. The remaining segments have no network

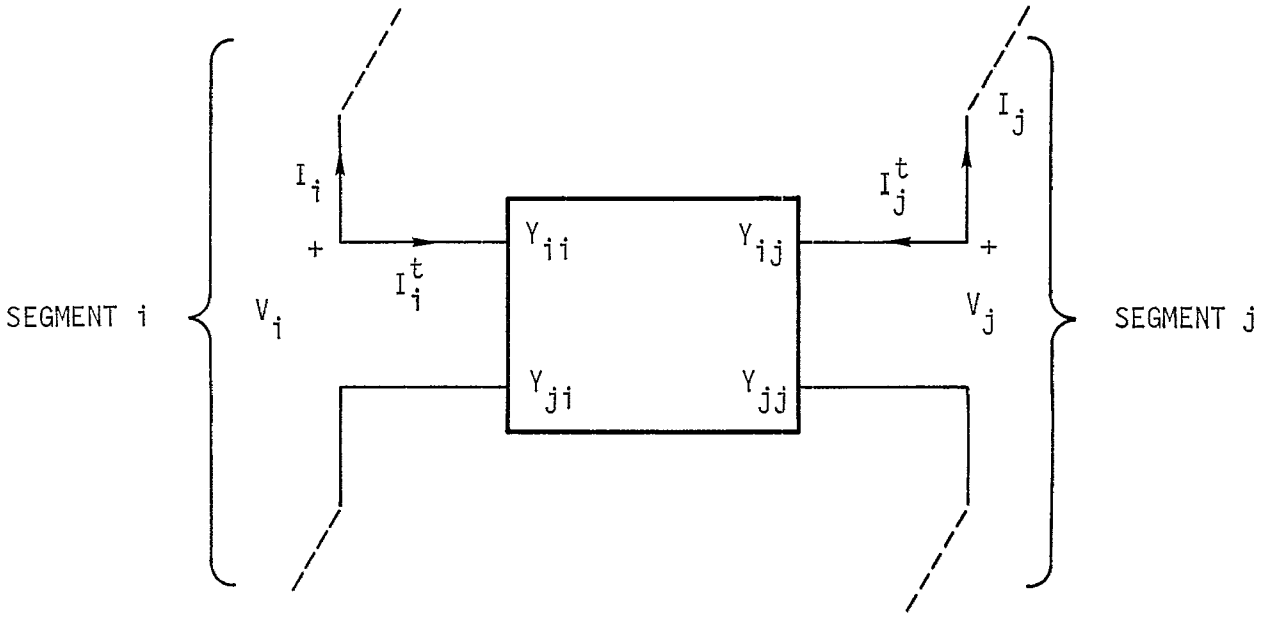

Figure 8. Network Connection to Segments.

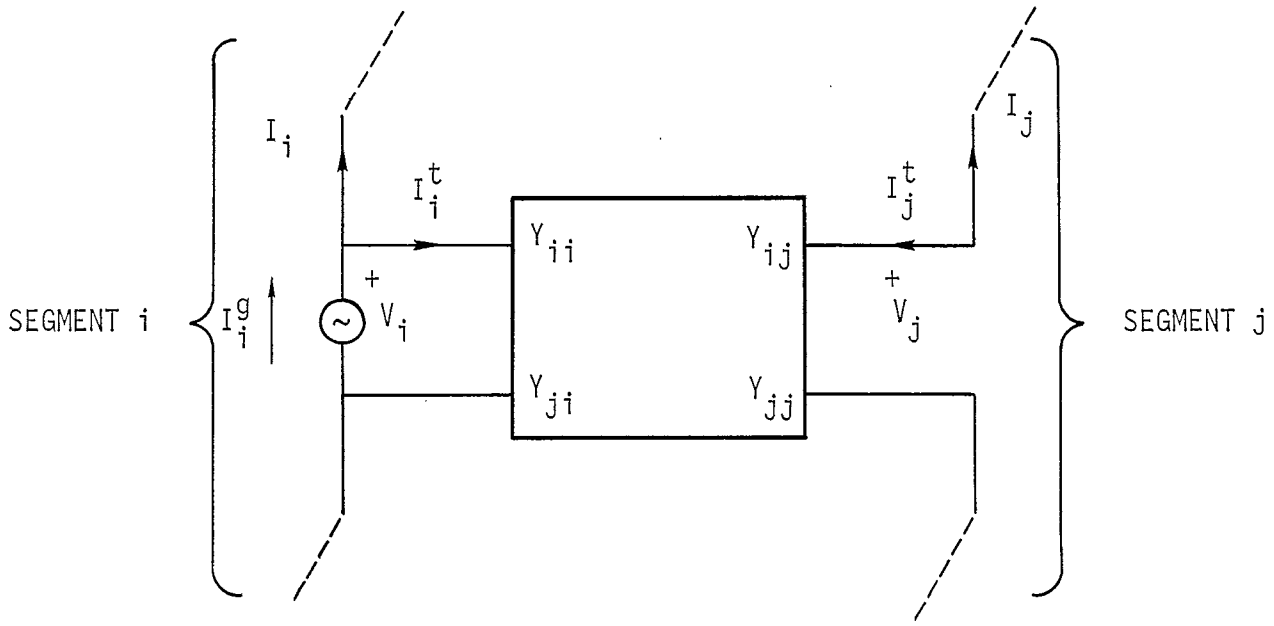

Figure 9. Network Port and Voltage Source Connected to a Segment.

connections but may have voltage sources. In addition all of the segments may be excited by an incident field represented by E_i^I on segment i. The total field on segment i is then

$$E_i = \frac{V_i}{\Delta_i} + E_i^I \ ,$$

where V_i is a gap voltage, due either to a network port or voltage source, and Δ_i is the segment length.

Equation (104) may be solved for current as

$$I_i = - \sum_{j=1}^{N_s} G_{ij}^{-1} E_j \qquad i=1, \ \ldots, \ N_s \ , \tag{108}$$

where G_{ij}^{-1} is the $(i,j)^{th}$ element of the inverse of matrix G. Before evaluating equation (108), however, the unknown port voltages, V_i, for $i = 1,\ldots,M_1$ must be determined. Hence, equation (108) is written with all known quantities on the right-hand side as

$$\sum_{j=1}^{M_1} G_{ij}^{-1} E_j^P + I_i = B_i \qquad i=1, \ \ldots, \ M_1 \ , \tag{109}$$

where

$$E_j^P = \frac{V_j}{\Delta_j} ,$$

and

$$B_i = - \sum_{j=1}^{M_1} G_{ij}^{-1} E_j^I - \sum_{j=M_1+1}^{N_s} G_{ij}^{-1} E_j .$$

Similarly, the network equations (105) are written using equation (106) as

$$\sum_{j=1}^{M_1} Y'_{ij} E_j^P + I_i = C_i \qquad i=1, \ldots, M_1 , \tag{110}$$

where

$$Y'_{ij} = \Delta_j Y_{ij} ,$$

$$C_i = - \sum_{j=M_1+1}^{M} Y_{ij} V_j .$$

The current is then eliminated between equations (109) and (110) to yield

$$\sum_{j=1}^{M_1} \left(G_{ij}^{-1} - Y'_{ij} \right) E_j^P = B_i - C_i \qquad i=1, \ldots, M_1 . \tag{111}$$

The solution procedure is then to solve equation (111) for E_j^P for $j = 1,\ldots,M_1$. Then, with the complete excitation vector determined, use equation (108) to determine I_i for $i = 1,\ldots,N_s$. Finally, the remaining network equations with equation (107) are used to compute the generator currents as

$$I_i^g = \sum_{j=1}^{M} Y_{ij} V_j + I_i \qquad i=M_1+1, \ldots M . \tag{112}$$

The currents I_i^g determine the input admittances seen by the sources.

In NEC the general M-port network used here is restricted to multiple two-port networks, each connecting a pair of segments.

3. TRANSMISSION LINE MODELING

Transmission lines interconnecting parts of an antenna may be modeled either explicitly by including the transmission line wires in the thin-wire model, or implicitly by the method described in the preceding section for nonradiating networks. For an implicit model, the short-circuit-admittance parameters of the transmission line viewed as a two-port network are

$$Y_{11} = Y_{22} = - j\, Y_o \cot(k\ell) ,$$

$$Y_{12} = Y_{21} = j\, Y_o \csc(k\ell) ,$$

where Y_o is the characteristic admittance of the line, k is the wave number $(2\pi/\lambda)$, and ℓ is the length of the line. If a separate admittance element is connected across the end of a transmission line, its admittance is added to the self-admittance of that network port.

The implicit model is limited, however, in that it neglects interaction between the transmission line and the antenna and its environment. This approximation is justified if the currents in the line are balanced, i.e., in a log periodic dipole antenna, and in general if the transmission line lies in an electric symmetry plane. The balance can be upset, however, if the transmission line is connected to an unbalanced load or by unsymmetric interactions. If the unbalance is significant, the transmission line can be modeled explicitly by including the wires in the thin wire model. The explicit model is completely general, and yields accurate results since the sine, cosine, and constant current expansion in NEC is a good representation of the sinusoidal transmission line currents. The accuracy is demonstrated in figure 10 for transmission lines terminated in short circuit, open circuit, and matched loads.

The explicit transmission line model is, of course, less efficient in computer time and storage because of the additional segments required. In cases where the physical line presence does have a significant effect on the results, the effect may be modeled by explicitly modeling a single conductor of the line while using the implicit model to represent the balanced current component.

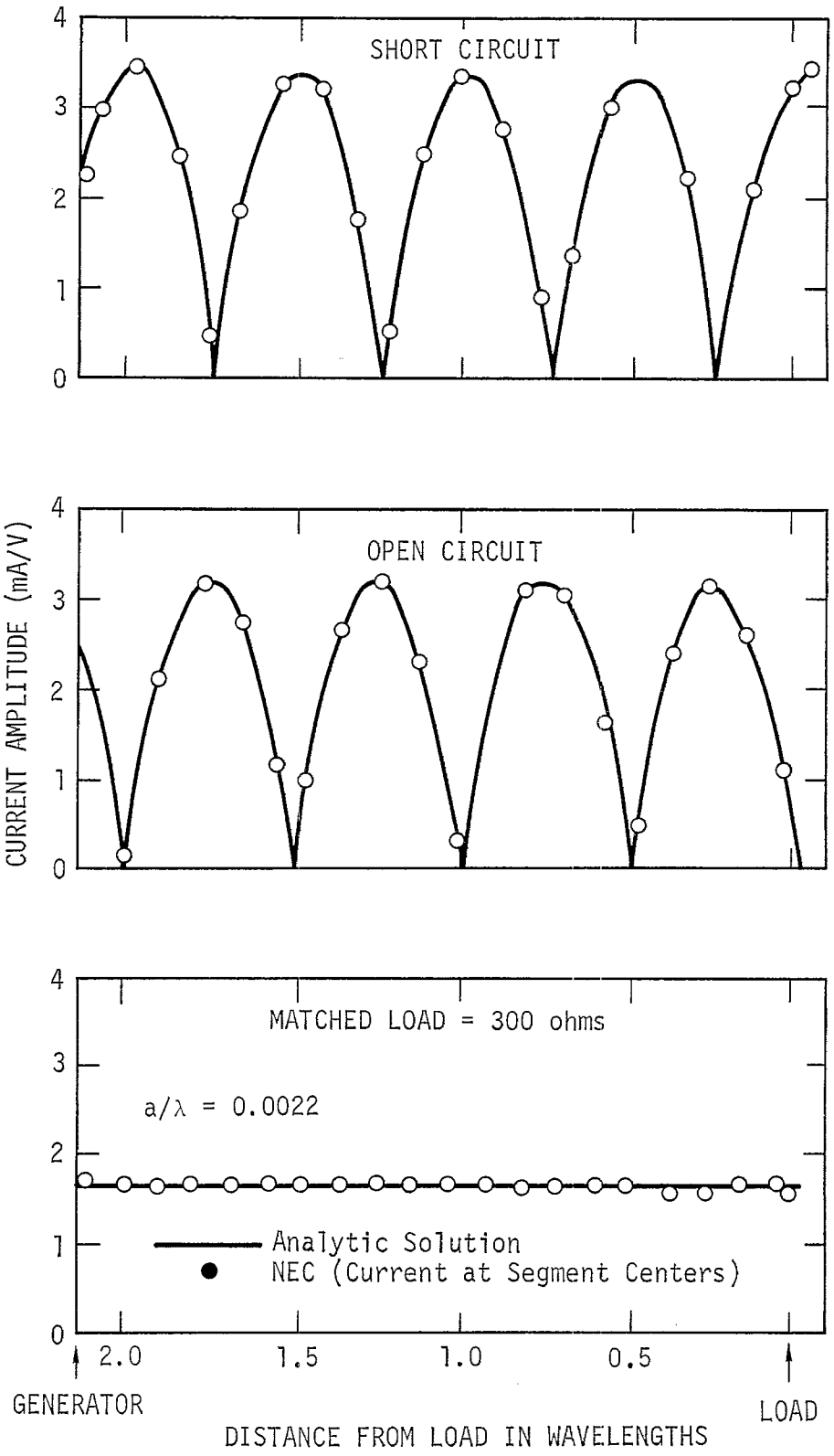

Figure 10. Current Distribution on a Two-Wire Transmission Line from NEC Compared with the Ideal Transmission Line Solution.

4. LUMPED OR DISTRIBUTED LOADING

Thus far, we have assumed that all structures to be modeled are perfect electric conductors. The EFIE is easily extended to imperfect conductors by modifying the boundary condition from equation (4) to

$$\hat{n}(\vec{r}) \times \left[\vec{E}^s(\vec{r}) + \vec{E}^I(\vec{r}) \right] = Z_s(\vec{r}) \left[\hat{n}(\vec{r}) \times \vec{J}_s(\vec{r}) \right] ,$$

where $Z_s(\vec{r})$ is the surface impedance at $\vec{r}$ on the conducting surface. For a wire, the boundary condition is

$$\hat{s} \cdot \left[\vec{E}^s(\vec{r}) + \vec{E}^I(\vec{r}) \right] = Z_w(s)\ I(s) ,$$

with $\vec{r}$ and $\hat{s}$ the position vector and tangent vector at s on the wire and $Z_w(s)$ the impedance per-unit-length at s. The matrix equation can then be written,

$$\sum_{j=1}^{N_s} G_{ij}\ \alpha_j = -\ E_i + \frac{Z_i}{\Delta_i} I_i \qquad i=1, \ldots, N_s , \tag{113}$$

where

α_j = amplitude of basis function j,

E_i = the incident field on segment i,

I_i = current at the center of segment i,

Z_i = total impedance of segment i,

Δ_i = length of segment i.

The impedance term can be viewed as a constant field model of a voltage source, as described in section IV-1, where the voltage is proportional to current. It is assumed that the current is essentially constant, with value I_i, over the length of the segment, which is a reasonable assumption for the electrically short segments used in the integral equation solution.

The impedance term can be combined with the matrix by expressing I_i in terms of the α_j as

$$I_i = \sum_{j=1}^{N_s} \alpha_j \left(A_j^i + C_j^i \right) ,$$

where A_j^i and C_j^i are the coefficients of the constant and cosine terms, respectively, in the section of basis function j extending onto segment i. If basis function j does not extend onto segment i, then A_j^i and C_j^i are zero. The matrix equation modified by loading is then

$$\sum_{j=1}^{N_s} G'_{ij} \alpha_j = - E_i \qquad i=1, \ldots, N_s , \tag{114}$$

where

$$G'_{ij} = G_{ij} - \frac{Z_i}{\Delta_i} \left(A_j^i + C_j^i \right) . \tag{115}$$

For a lumped circuit element, Z_i is computed from the circuit equations. For a distributed impedance, Z_i represents the impedance of a length Δ_i of wire, which in the case of a round wire of finite conductivity is given by

$$Z_i = \frac{j\Delta_i}{a_i} \sqrt{\frac{\omega\mu}{2\pi\sigma}} \left[\frac{\mathrm{Ber}(q) + j\ \mathrm{Bei}(q)}{\mathrm{Ber}'(q) + j\ \mathrm{Bei}'(q)} \right] ,$$

where

$q = (\omega\mu\sigma)^{1/2}\ a_i$,

a_i = wire radius,

σ = wire conductivity,

Ber, Bei = Kelvin functions.

This expression takes account of the limited penetration of the field into an imperfect conductor.

5. RADIATED FIELD CALCULATION

The radiated field of an antenna or reradiated field of a scatterer can be computed from the induced current by using a simplified form of equation (1) valid far from the current distribution. The far-field approximation, valid when the distance from the current distribution to the observation

point is large compared to both the wavelength and the dimensions of the current distribution, treats the distance $|\vec{r} - \vec{r}'|$ as constant within the integral except in the phase term, $\exp(-jk|\vec{r} - \vec{r}'|)$. For a structure consisting of a wire portion with contour L and current distribution $\vec{I}(s)$, and a surface portion S with current $\vec{J}_s(\vec{r})$, the far-zone field is

$$\vec{E}(\vec{r}_o) = \frac{jk\eta}{4\pi} \frac{\exp(-jkr_o)}{r_o} \left\{ \int_L \left[\left(\hat{k} \cdot \vec{I}(s) \right) \hat{k} - \vec{I}(s) \right] \exp(j\vec{k}\cdot\vec{r}) ds + \int_S \left[\left(\hat{k}\cdot\vec{J}_s(\vec{r}) \right) \hat{k} - \vec{J}_s(\vec{r}) \right] \exp(j\vec{k}\cdot\vec{r}) dA \right\} , \quad (116)$$

where $\vec{r}_o$ is the position of the observation point $\hat{k} = \vec{r}_o / |\vec{r}_o|$, $k = 2\pi/\lambda$, and $\vec{k} = k\hat{k}$. The first integral can be evaluated in closed form over each straight wire segment for the constant, sine, and cosine components of the basis functions, and reduces to a summation over the wire segments. With the surface current on each patch represented by a delta function at the patch center, the second integral becomes a summation over the patches.

The radiation pattern of an antenna can be computed by exciting the antenna with a voltage source and using equation (116) to compute the radiated field for a set of directions in space. Alternatively, since the transmitting and receiving patterns are required by reciprocity to be the same, the pattern can be determined by exciting the antenna with plane-waves incident from the same directions and computing the currents at the source point. The solution procedure in NEC does not guarantee reciprocity, however, since the different expansion and weighting functions may produce asymmetry in the matrix. Large differences between the receiving and transmitting patterns or a significant lack of reciprocity in bistatic scattering are indications of inaccuracy in the solution, possibly from too coarse a segmentation of the wires or surfaces.

The power gain of an antenna in the direction specified by the spherical coordinates (Θ,ϕ) is defined as

$$G_p(\Theta,\phi) = 4\pi \frac{P(\Theta,\phi)}{P_{in}} ,$$

35). For example, the z component of electric field due to a vertical current element is

$$E_z^v = -j\eta Id\ell/2\lambda \left\{ \cos^2 \psi' \; e^{-jkR_1}/R_1 + R_v \cos^2 \psi \right.$$

$$e^{-jkR_2}/R_2 + (1-R_v)(1-u^2 + u^4 \cos^2 \psi) F \; e^{-jkR_2}/R_2$$

$$+ u\sqrt{1-u^2 \cos^2 \psi} \sin \psi \; 2 \; e^{-jkR_2}/jkR_2^2$$

$$+ e^{-jkR_1}/R_1 \left(1/jkR_1 + 1/(jkR_1)^2\right) (1-3 \sin^2 \psi')$$

$$\left. + e^{-jkR_2}/R_2 \left(1/jkR_2 + 1/(jkR_2)^2\right) (1-3 \sin^2 \psi) \right\} ,$$

where

$F = 1-j\sqrt{\pi\omega}\, e^{-\omega}\, \mathrm{erfc}(j\sqrt{\omega})$,

$\mathrm{erfc}(\;\;)$ = error function,

$\omega = 4p_1/(1-R_v)^2$,

$p_1 = -jkR_2u^2(1-u^2 \cos^2 \psi)/2$,

$R_v = (\sin \psi - u\sqrt{1-u^2 \cos^2 \psi}) / (\sin \psi + u\sqrt{1-u^2 \cos^2 \psi})$,

$u = k/k_2$,

k = free-space wave number,

k_2 = wave number in lower medium,

$\sin \psi = (z + a)/R_2$,

$\sin \psi' = (z - a)/R_1$,

a = height of current element above ground,

z = height of observer above ground,

R_1 = distance from current element to observer,

R_2 = distance from image of current element to observer.

where $P(\Theta,\phi)$ is the power radiated per unit solid angle in the direction (Θ,ϕ), and P_{in} is the total power accepted by the antenna from the source. P_{in} is computed from the voltage and current at the source as

$$P_{in} = \frac{1}{2} \mathrm{Re}(VI^*) ,$$

and

$$P(\Theta,\phi) = \frac{1}{2} R^2 \mathrm{Re}(\vec{E} \times \vec{H}^*) = \frac{R^2}{2\eta} (\vec{E} \cdot \vec{E}^*) .$$

$\vec{E}$ is obtained from equation (116) with $\vec{r}_o$ in the direction (Θ,ϕ), and $r_o = R$. Directive gain is similarly defined as

$$G_d(\Theta,\phi) = 4\pi \frac{P(\Theta,\phi)}{P_{rad}} ,$$

where P_{rad} is the total power radiated by the antenna,

$$P_{rad} = P_{in} - P_{loss} ,$$

and P_{loss} is the total ohmic loss in the antenna.

6. GROUND-WAVE FIELD

The radiated field of an antenna over ground is modified by the ground interaction, as discussed in section II-4. When the range from the antenna to the observer, R, approaches infinity, the Sommerfeld formulation for the field reduces exactly to a direct field determined by equation (116) and a field from the image modified by the Fresnel reflection coefficient. In some cases, however, when the observer is at a finite distance from the antenna, the field components proportional to $1/R^2$ may be significant. While the $1/R$ terms are generally much larger than the $1/R^2$ terms at practical observation distances from an antenna, the $1/R$ terms vanish at grazing angles over an imperfect ground plane leaving only the $1/R^2$ terms, dominated by a term known as the ground wave. The ground wave is, of course, included in Sommerfeld's expressions. However, it is more easily evaluated from closed-form approximations.

A set of approximate expressions for the field of differential current elements of vertical or horizontal orientation were derived by Norton (ref.

Expressions for the other field components of a vertical or horizontal current element are given in Norton's paper. The field of an arbitrarily oriented current element can be obtained from these expressions by decomposing the current element into horizontal and vertical components and applying appropriate coordinate transformations. The approximations involved in these expressions are valid for R greater than a few wavelengths and to second order in u^2. The second condition is satisfied for practical ground media. When the ground wave is included, the field has radial as well as transverse components.

Section V
Validating Results

Some results are presented in this section to demonstrate the range of validity of the NEC code. The results include antennas over a ground plane, showing the range of validity of the reflection-coefficient approximation, and a solid cylinder with wires attached. For simple wire antennas, the code has been thoroughly tested and found to be highly accurate. Some situations have been found to result in reduced accuracy, however. These include large, abrupt changes in wire radius and structures very small relative to the wavelength. Methods of modeling such antennas are discussed in other reports (refs. 36, 37 and 38), which include comparisons with measured data taken at the Naval Ocean Systems Center.

1. ANTENNAS OVER GROUND

In most cases data obtainable by independent analytical techniques are not sufficiently accurate to serve as a useful check on NEC. For an antenna over ground, however, the Sommerfeld integral formulas provide a good check of the reflection-coefficient approximation since Sommerfeld's formulas are valid for any ground parameters and interaction distance. Both methods use the same integral-equation-solution technique, which is highly accurate for the simple structures considered here.

Figure 11 illustrates the input resistance of a vertical half-wave dipole as a function of height over a lossy ground. The comparison with the Sommerfeld integral results points out that significant discrepancies occur only when the dipole is very close to the ground and that even when the tip is touching, an error of less than 10% is encountered. The input resistance of a 0.1λ horizontal dipole above a dielectric half-space is shown as a function of height above ground in figure 12. Comparison with the scant, independent data indicates close agreement. A comparison with experimental data for a purely dielectric ground is shown in figure 13. The plot pertains to the input resistance of a horizontal half-wave dipole as a function of its height above ground. Since the antenna radiation pattern is also of great interest, we include in figure 14 the radiation patterns of a monopole over a dielectric ground. The results are compared to those presented by Wait (ref. 24) wherein a current distribution on the monopole was assumed. For comparison, a Sommerfeld integral calculation is also provided. The NEC data have been

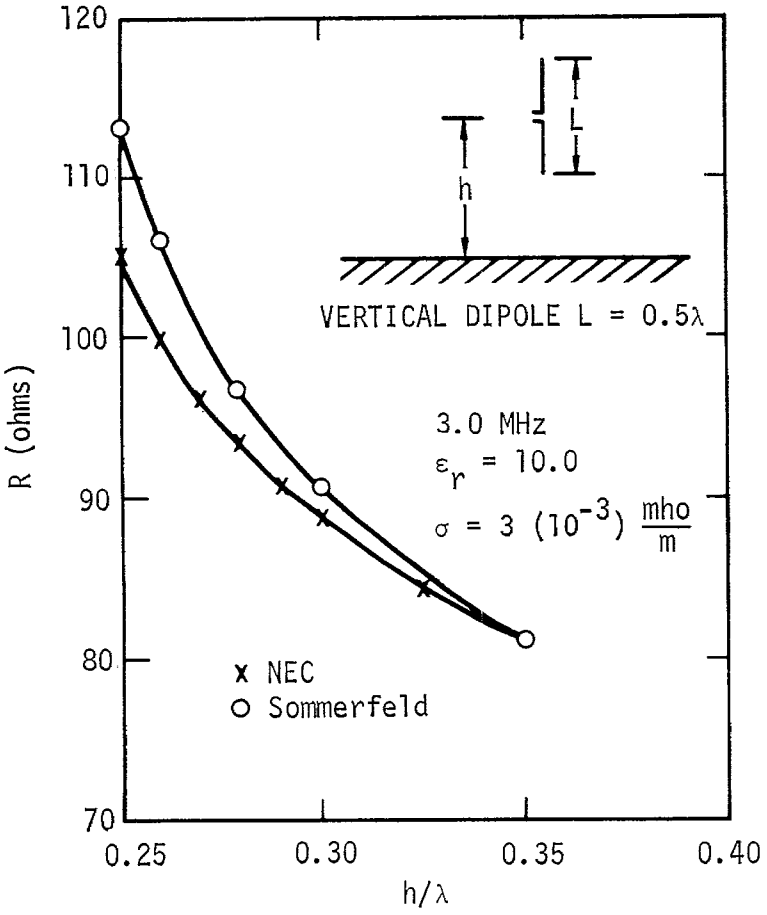

Figure 11. Input Resistance of a Half-Wave Dipole Over a Lossy Ground at 3 MHz.

normalized to Wait's data and the same normalization factor applied to the Sommerfeld data. The input resistance and radiation patterns of an array of two vertical dipoles, one driven and one parasitic, at various heights above ground are compared in figure 15. The input resistance versus dipole separation is shown in figure 16.

These results indicate that the reflection-coefficient approximation can provide usefully accurate results for a wide range of cases involving antennas over ground. There are cases, however, for which the approximation breaks down. Although figure 11 indicates reasonable accuracy for a vertical dipole antenna when the tip touches the ground, large errors may occur for a vertical monopole antenna on an imperfect ground. A practical monopole antenna, however, is usually fed against a ground screen or some other grounding device. Hence, rather than feeding the monopole against the imperfect ground, a more realistic model in NEC might employ a radial-wire ground screen or perfectly conducting ground in the vicinity of the monopole. This

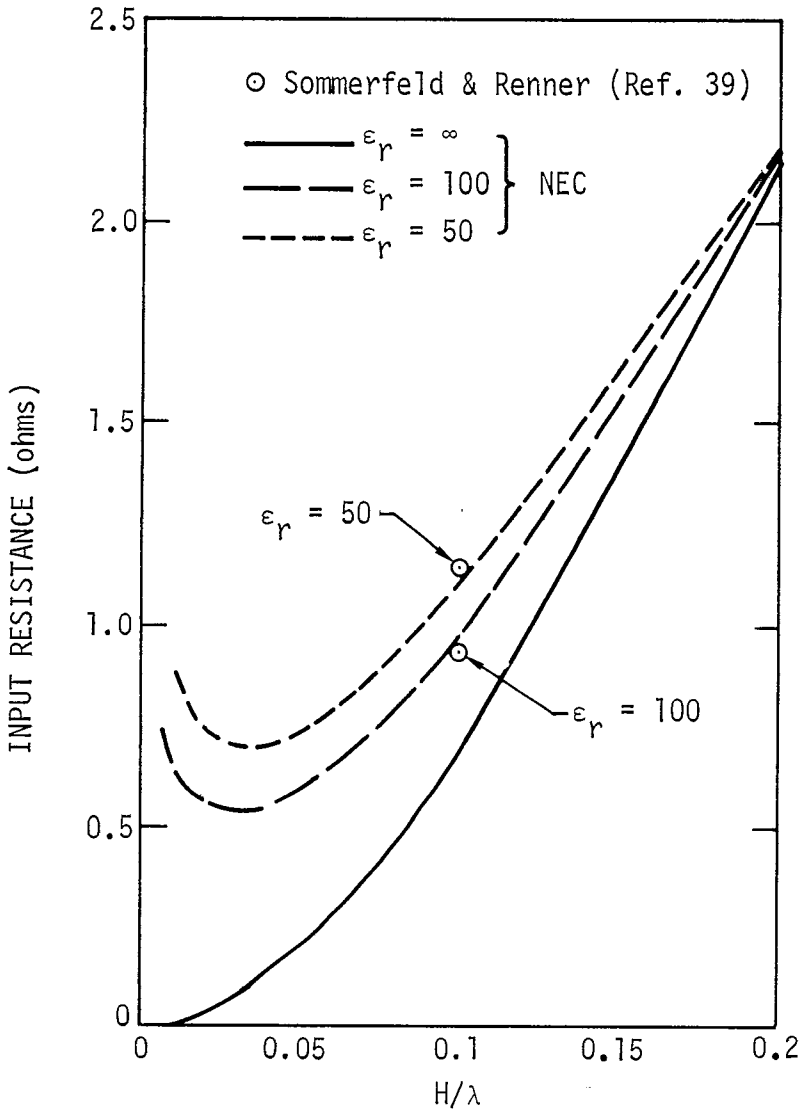

Figure 12. Input Resistance of a Horizontal Dipole, 0.1 λ Long, Located a Distance H above a Purely Dielectric Ground (Dielectric Constant ε_r).

avoids the inaccuracy in feeding against an imperfect ground. The reflection-coefficient approximation is also inaccurate for interactions between wires close to the ground where the reflecting ray has grazing incidence on the imperfect ground, a case which occurs in the Beverage antenna.

2. CYLINDER WITH ATTACHED WIRES

To demonstrate the validity of NEC for modeling combined wire and surface structures, three comparisons of computed and experimental radiated-field patterns are presented in figures 17, 18, and 19. The experimental data are from a set of measurements taken at the University of Denmark by Albertsen et al. (ref. 9) of spacecraft-like models. Albertsen et al. compared these

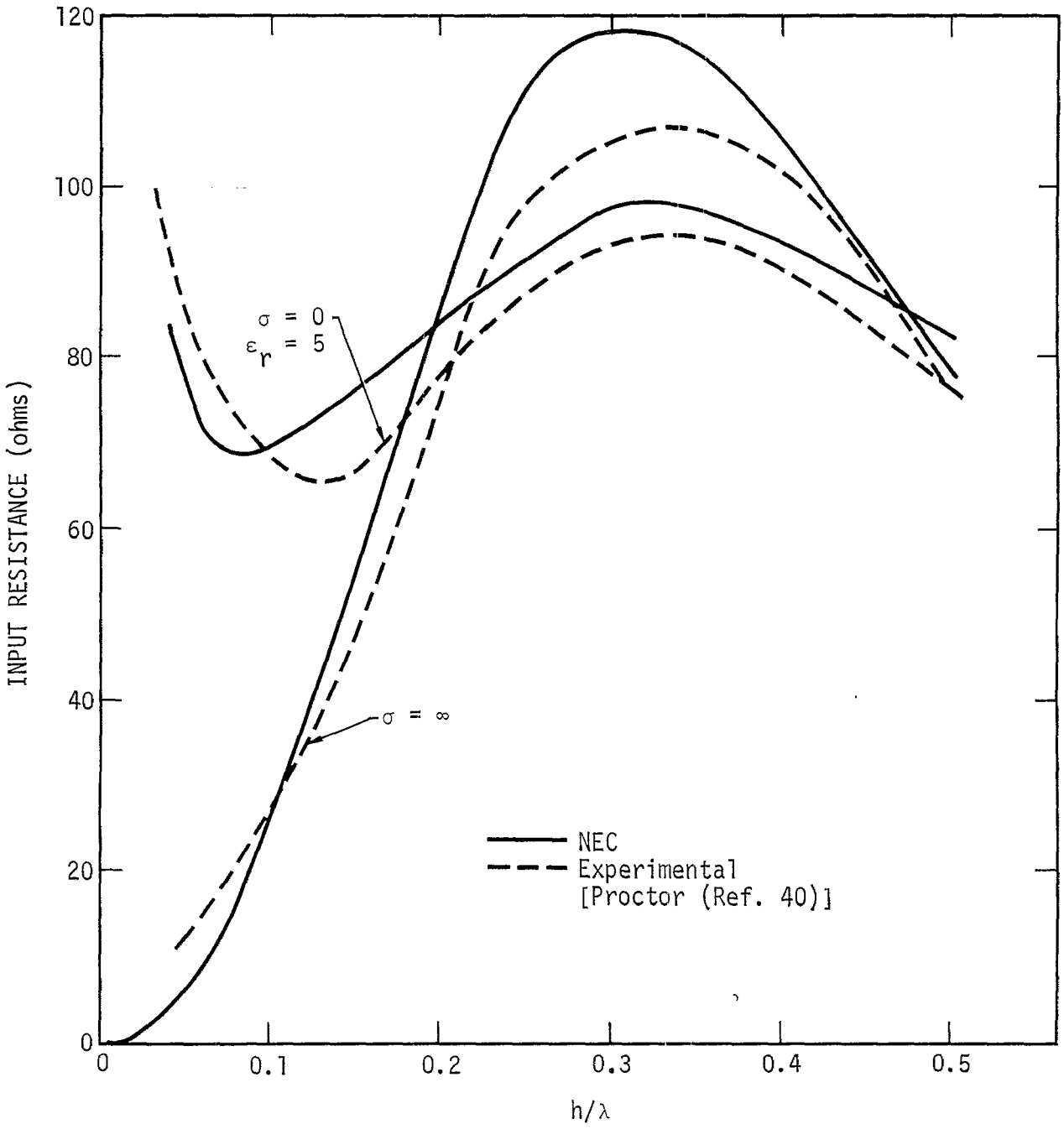

Figure 13. Input Resistance of a Horizontal Half-Wave Dipole Located a Distance h above a Purely Dielectric Ground, ε_r = s.

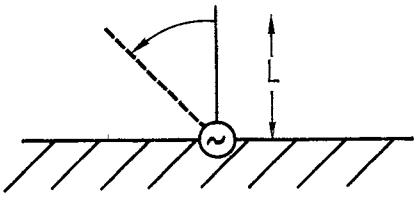

MONOPOLE LENGTH = L

$\varepsilon_r = 4.0$

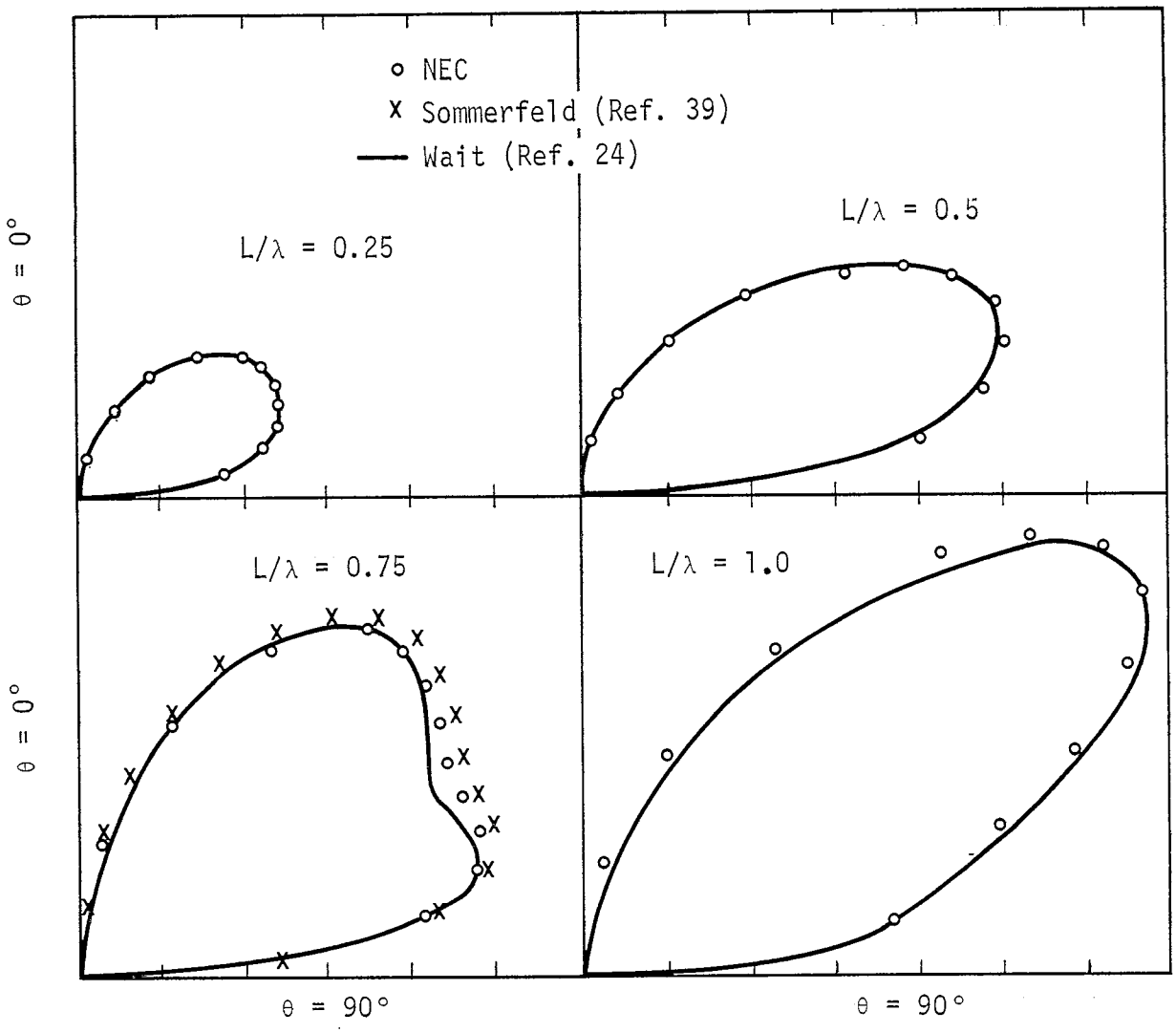

Figure 14. Radiation Patterns (Linear Voltage Scale) of a Monopole over a Dielectric Ground.

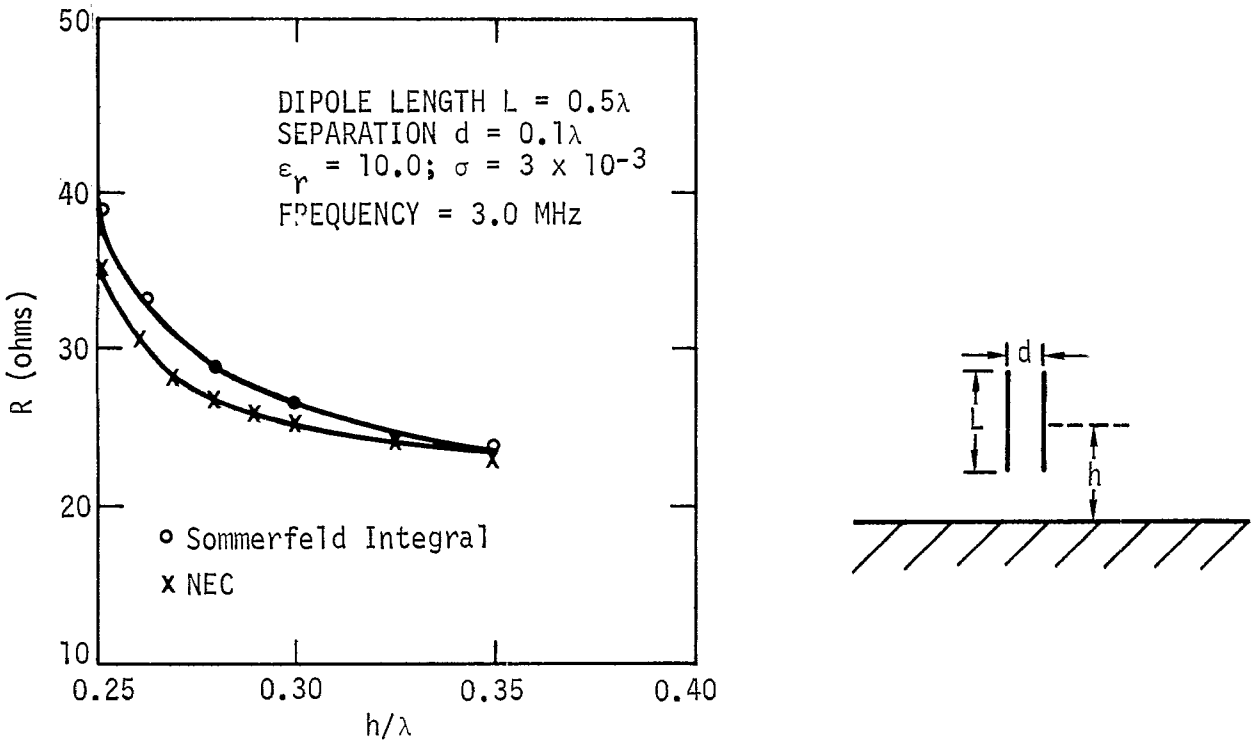

a) Input Impedance

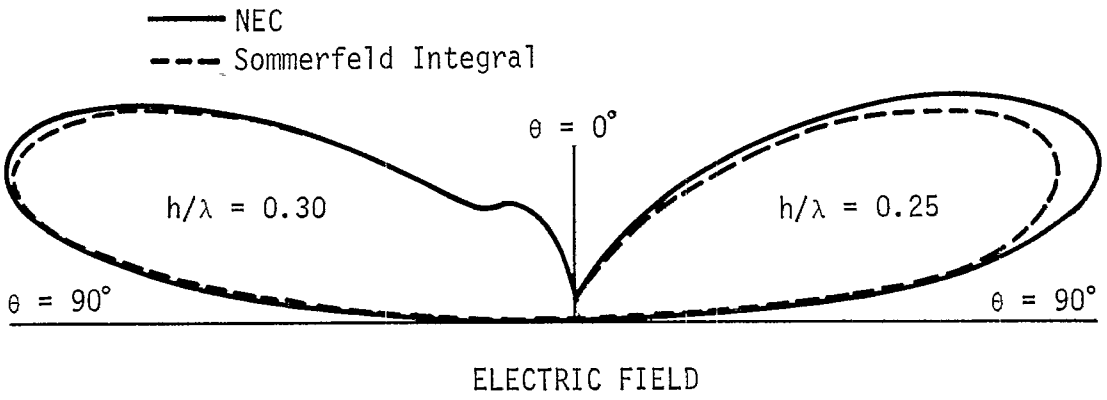

b) Radiation Patterns

Figure 15. Input Impedance and Radiation Patterns for a Parasitic Array of Two Half-Wave Dipoles.

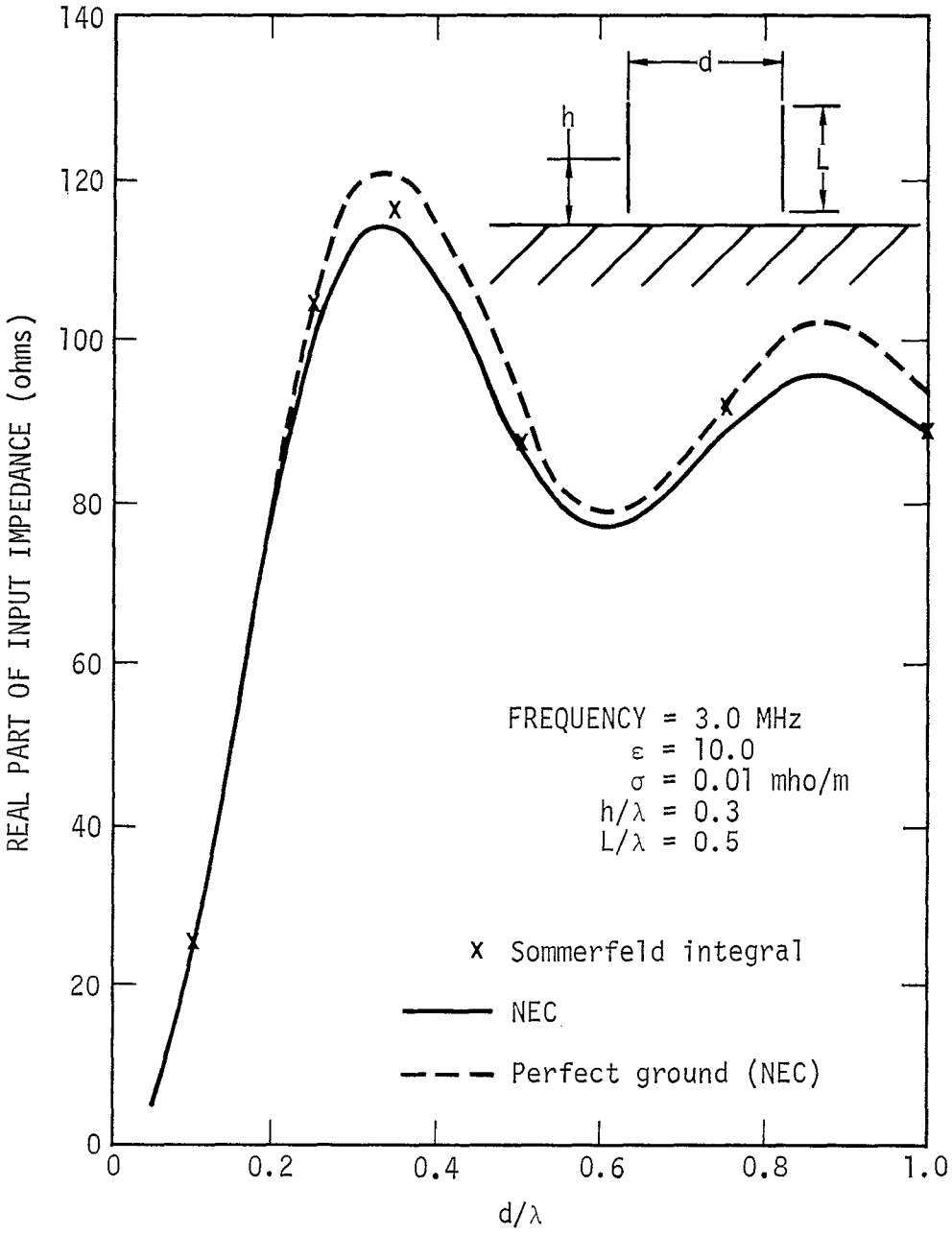

Figure 16. Input Resistance for a Parasitic Array of Two Half-Wave Dipoles.

measurements with results of their own computer program after which the treatment of the connection of a wire to a surface in NEC is patterned.

In each case the structure is a 22-cm-high cylinder with a 20-cm diam. Two wires are attached in various locations on the cylinder as illustrated in the upper right hand corners of figures 17, 18, and 19. These illustrations also show, by a small test dipole, the plane of the radiation pattern and

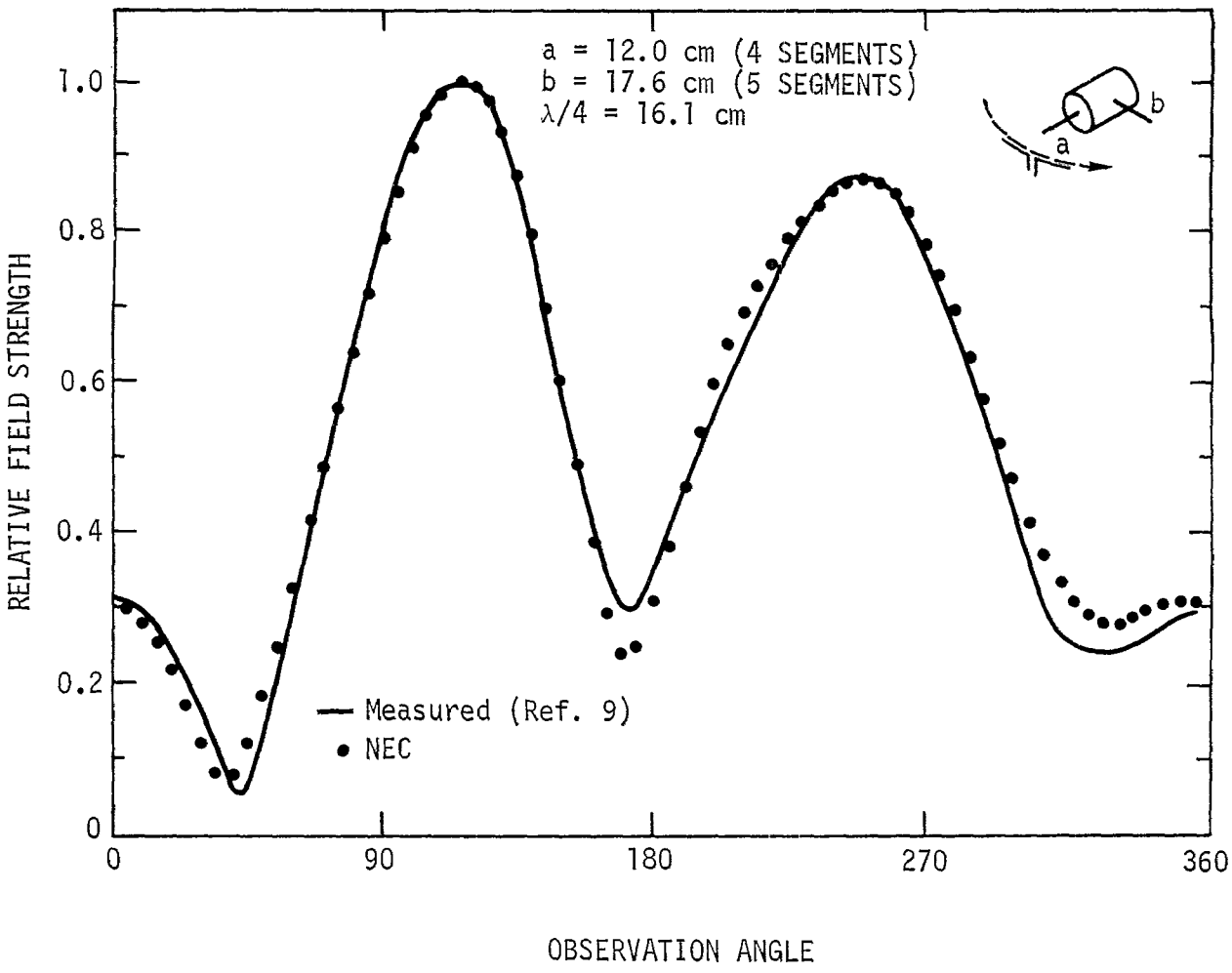

Figure 17. Experimental/Numerical Radiation Pattern of Cylinder with Attached Wires.

the position of zero degrees in observation angle. The division of the cylinder into patches is the same in each case except for the subdivision at the points where the wires connect. The segmentation of the cylinder for the wire connection of figure 17 is shown in figure 20. The shape drawn for each patch is only for the purpose of illustration since the program only uses the patch center-point and area. In each case, wire a is driven against the cylinder by a voltage source at its base while wire b is connected directly to the cylinder.

The agreement of the computations with the measurement is about the same as was obtained by Albertsen et al. The worst agreement is for the case of figure 18. This agreement is slightly worse than was obtained with the

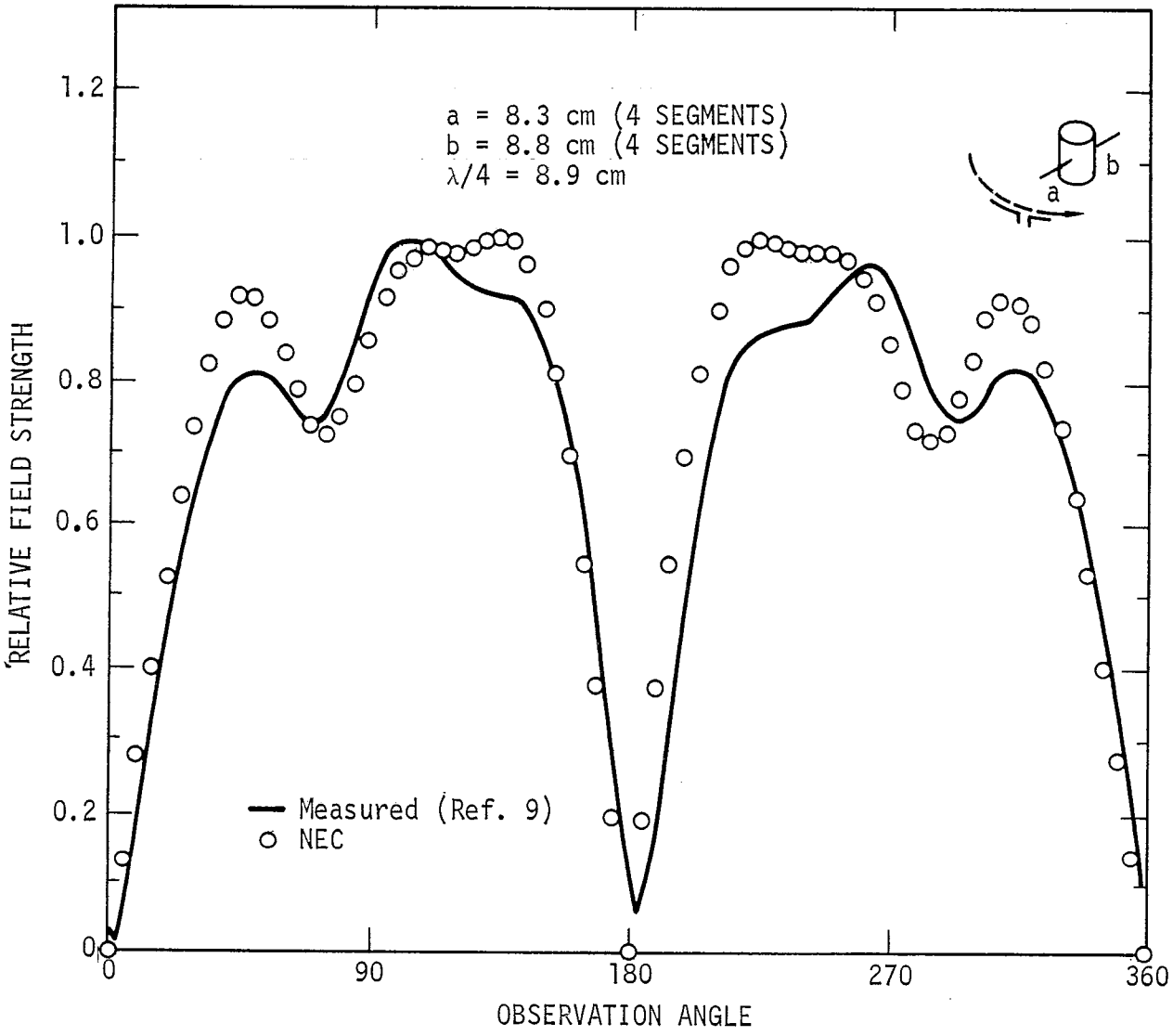

Figure 18. Experimental/Numerical Radiation Pattern of Cylinder with Attached Wires.

earlier program AMP2 despite several refinements in NEC. The agreement is also worse than that obtained by Albertsen et al. This appears to be a particularly unstable pattern, however, since when the number of segments on each wire is increased from 4 to 5, the agreement with measurement becomes worse with either NEC or AMP2. No special consideration has been given to the edges of the cylinder although increased patch density near the edges might improve the results. Generally, the agreement is good, however, and was obtained with considerably less computation time than would be required with a wire-grid model of the cylinder.

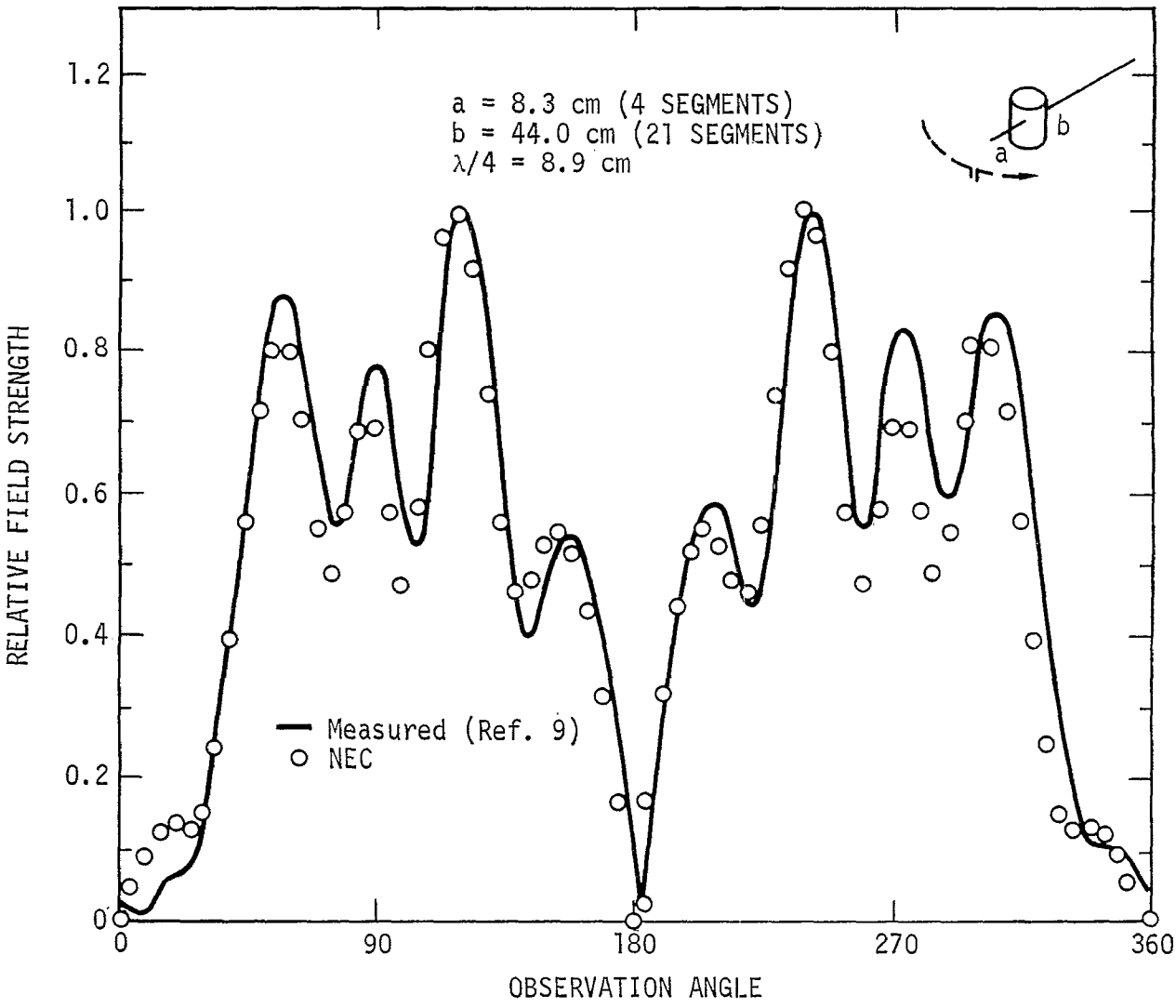

Figure 19. Experimental/Numerical Radiation Pattern of Cylinder with Attached Wires.

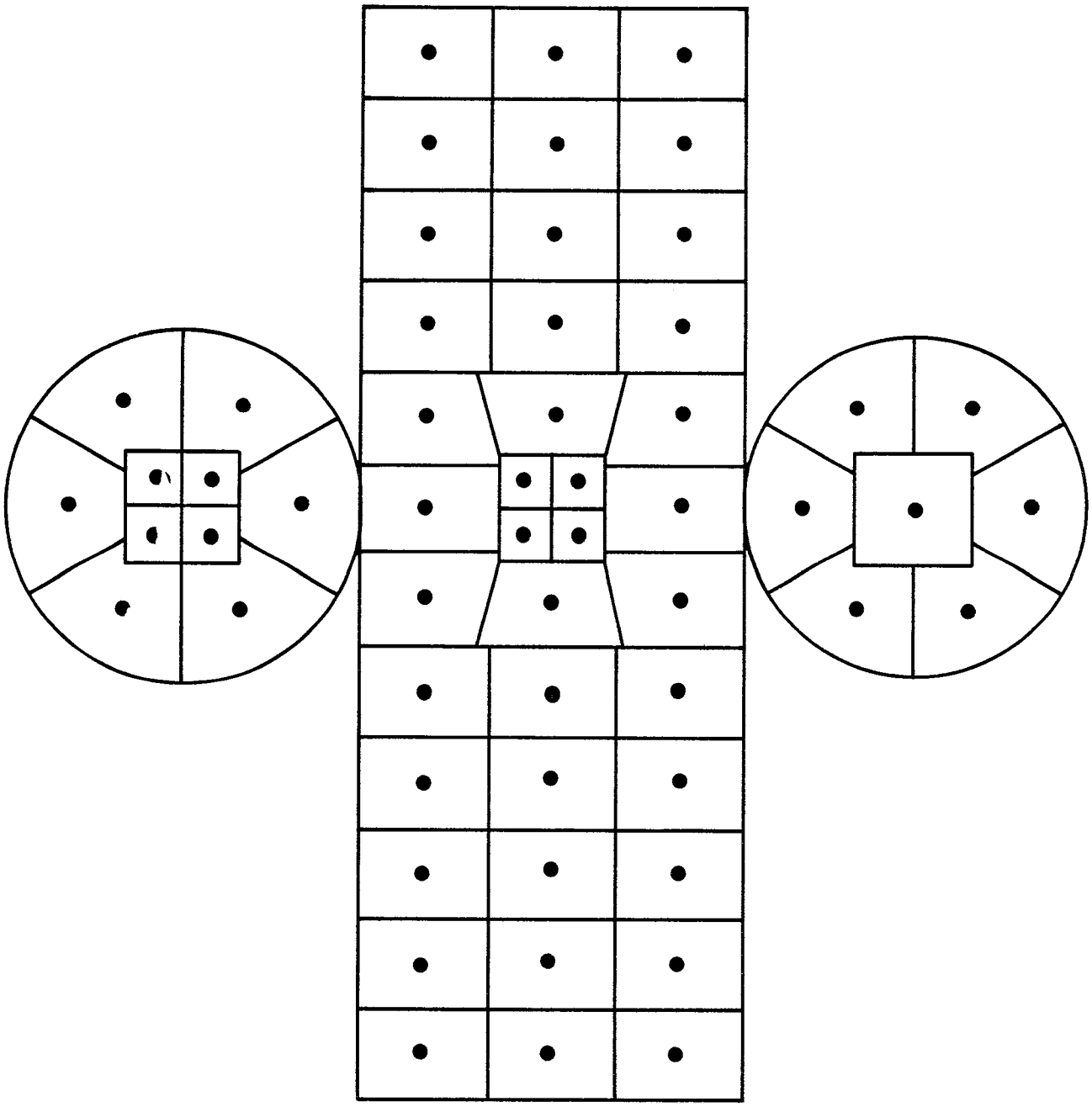

Figure 20. Segmentation of Cylinder for Wires Connected to End and Side.

References

1. Miller, E. K. et al., *Final Technical Report on the Log-Periodic Scattering Array Program,* MBAssociates Report No. MB-R-70/105, Contract No. F04701-68-C-0188, 1970.
2. *RCS Computer Program BRACT, Log-Periodic Scattering Array Program - II,* MBAssociates Report No. MB-R-69/46, Contract No. F04701-68-C-0188, 1969.
3. *Antenna Modeling Program - Composite User's Manual,* MBAssociates Report No. MB-R-74/46, 1974.
4. *Antenna Modeling Program - Engineering Manual,* MBAssociates Report No. MB-R-74/62, 1974.
5. *Antenna Modeling Program - Systems Manual,* MBAssociates Report No. MB-R-74/62, 1974.
6. *Antenna Modeling Program, Supplementary Computer Program Manual (AMP2),* MBAssociates Report No. MB-R-75/4, 1975.
7. Numerical Electromagnetic Code (NEC(1,2)A), Volume II: User's Guide, Interaction Application Memo 31, July 1977.
8. Numerical Electromagnetic Code (NEC(1,2)A), Volume III: Program Description Code, Interaction Application Memo 32, July 1977.
9. Albertsen, N. C., Hansen, J. E., and Jensen, N. E., *Computation of Spacecraft Antenna Radiation Patterns,* The Technical University of Denmark, Lyngby, Denmark, June 1972.
10. Poggio, A. J. and Miller, E. K., "Integral Equation Solutions of Three-Dimensional Scattering Problems," Chapt. IV in *Computer Techniques for Electromagnetics,* edited by R. Mittra, Pergamon Press, New York, 1973.
11. Poggio, A. J. and Adams, R. W., *Approximations for Terms Related to the Kernel in Thin-wire Integral Equations,* Mathematics Note 44, January 1977.
12. Van Bladel, J., *Electromagnetic Fields,* McGraw-Hill, New York, 1964.
13. Sommerfeld, A., *Partial Differential Equations in Physics,* Academic Press, New York, 1964.
14. Burke, G. J., Miller, E. K., and Poggio, A. J., *Dielectric Ground Interactions with a Log-Periodic Antenna,* Final Report, ECOM-0285-F, U.S. Army Electronics Command, Fort Monmouth, N.J., 1971 (contract DAAB07-70-C-0285).

15. Miller, E. K., Poggio, A. J., Burke, G. J., and Selden, E. S., *Analysis of Wire Antennas in the Presence of a Conducting Half Space: Part I. The Vertical Antenna in Free Space. Part II. The Horizontal Antenna in Free Space,* UCRL-73217, Lawrence Livermore Laboratory, CA, 1972. (Also in *Canadian J. Phys.)*

16. Banos, A., Jr., *Dipole Radiation in the Presence of a Conducting Half-Space,* Pergamon Press, New York, 1966.

17. Siegel, M., *The Electromagnetic Fields of a Dipole in a Dissipative Half-Space: A Numerical Approach,* Harvard University Division of Engineering and Applied Physics, May, 1970.

18. Feynberg, Y. L., *The Propagation of Radio Waves Along the Surface of the Earth,* Foreign Technology Division, Wright-Patterson Air Force Base, Ohio, 1967.

19. Wait, J. R., Editor, *Conference on Environmental Effects on Antenna Performance,* Proceedings, Vol. 1, Boulder, Colorado, July 14-18, 1969.

20. Surtess, W. J., "Effects of the Ground Screen on the Field Radiated From a Monopole," *Proceedings of Conference on Environmental Effects on Antenna Performance,* Boulder, Colorado, Vol. 1, p. 95, 1969.

21. Wait, J. R., "Impedance of a Hertzian Dipole Over a Conducting Half-Space," *Conference on Environmental Effects on Antenna Performance,* Vol. 1, Boulder, Colorado, July 14-18, 1969.

22. Stratton, J. A., *Electromagnetic Theory,* McGraw-Hill, New York, 1941.

23. Miller, E. K. and Deadrick, F. J., *Computer Evaluation of Loran-C Antennas,* URCL-51464, Lawrence Livermore Laboratory, CA, Oct. 17, 1973.

24. Wait, J. R., "Characteristics of Antennas Over Lossy Earth," *Antenna Theory, Part II,* R. E. Collin and F. J. Zucker, Eds., McGraw-Hill, New York, pp. 386-437, 1969.

25. Harrington, R. F., *Field Computation by Moment Methods,* MacMillan, New York, 1968.

26. Neureuther, A. R. et al., "A Comparison of Numerical Methods for Thin Wire Antennas," *Presented at the 1968 Fall URSI meeting,* Dept. of Electrical Engineering and Computer Sciences, University of California, Berkeley, 1968.

27. Miller, E. K. et al., *An Evaluation of Computer Programs Using Integral Equations for the Electromagnetic Analysis of Thin Wire Structures*, and Interaction Note 177, March 1974.

28. Wu, T. T. and King, R. W. P., "The Tapered Antenna and Its Application to the Junction Problem for Thin Wires," *IEEE Trans. Ant. and Prop.*, *AP-24*, No. 1, pp. 42-45, January 1976, and also Interaction Note 269, January 1976.

29. Poggio, A. J., *Integral Representations for Fields Due to Sources on Open Surfaces with Applications to End Caps*, UCRL-51723, Lawrence Livermore Laboratory, CA, December 16, 1974.

30. Ralston, A., *A First Course in Numerical Analysis*, McGraw-Hill, New York, 1965.

31. King, R. W., *The Theory of Linear Antennas*, Harvard Univ. Press, Cambridge, Massachusetts, 1956.

32. Otto, D. V., "The Admittance of Cylindrical Antennas Driven from a Coaxial Line," *Radio Sci.*, Vol. 2, No. 9, pp. 1031-1042, 1967.

33. Andreasen, M. G. and Harris, F. G., *Analyses of Wire Antennas of Arbitrary Configuration by Precise Theoretical Numerical Techniques*, Tech. Rept. ECOM 0631-F, Granger Associates, Palo Alto, California, Contract DAAB07-67-C-0631, 1968.

34. Adams, R. W., Poggio, A. J., and Miller, E. K., *Study of a New Antenna Source Model*, UCRL-51693, Lawrence Livermore Laboratory, CA, October 28, 1974.

35. Norton, K. A., "The Propagation of Radio Waves Over the Surface of the Earth and in the Upper Atmosphere," *Proceedings of the Institute of Radio Engineers*, Vol. 26, No. 9, Sept. 1937.

36. Burke, G. J. and Poggio, A. J., *Computer Analysis of the Twin-Whip Antenna*, UCRL-52080, Lawrence Livermore Laboratory, CA, June 1, 1976.

37. Burke, G. J. and Poggio, A. J., *Computer Analysis of the Bottom-Fed Fan Antenna*, UCRL-52109 Lawrence Livermore Laboratory, CA, August 19, 1976.

38. Deadrick, F. J., Burke, G. J., and Poggio, A. J., *Computer Analysis of the Trussed-Whip and Discone-Cage Antennas*, UCRL-52201, January 6, 1977.

39. Sommerfeld, A. and Renner, F., *Strahlungsenergie Und Erdabsorption bei Dipolantennen*, Ann. Physik, Vol. 41, 1942.

40. Proctor, R. F., *Input Impedance of Horizontal Dipole Aerials at Low Heights Above the Ground*, J. Inst. Elect. Engrs. (London), Vol. 97, Part III, p. 133, 1950.

Appendix

FIELD EQUATIONS FOR THE KERNEL OF THE ELECTRIC FIELD INTEGRAL EQUATION

In the NEC code, an arbitrary wire structure is represented by a set of straight wire segments. Each has a current of the form

$$I_i(s) = A_i + B_i \sin k(s - s_i) + C_i \cos k(s - s_i) \qquad (A1)$$

$$|s - s_i| < \Delta_i/2 \ ,$$

where $k = \omega\sqrt{\mu\varepsilon}$, and Δ_i is the segment length. The solution requires the evaluation of the electric field at each segment due to this current. Three approximations of the integral equation kernel are used: a thin-wire form for most cases, an extended thin-wire form for thick wires, and a simplified thin wire form for large interaction distances. In each case the evaluation of the field is greatly simplified by the use of formulas for the fields of the constant and sinusoidal current components.

For the thin-wire kernel, the source current is approximated by a filament on the segment axis while the observation point is on the surface of the observation segment. The fields are evaluated with the source segment on the axis of a local cylindrical-coordinate system as illustrated in figure A1. Then with

$$G_o = \exp(-jkr_o)/r_o \ , \qquad (A2)$$

$$r_o = \left[\rho^2 + (z - z')^2\right]^{1/2} \ , \qquad (A3)$$

the ρ and z components of the electric field at P due to a sinusoidal current filament of arbitrary phase,

$$I = \sin(kz' - \Theta_o) \ , \ z_1 < z' < z_2 \ , \qquad (A4)$$

are

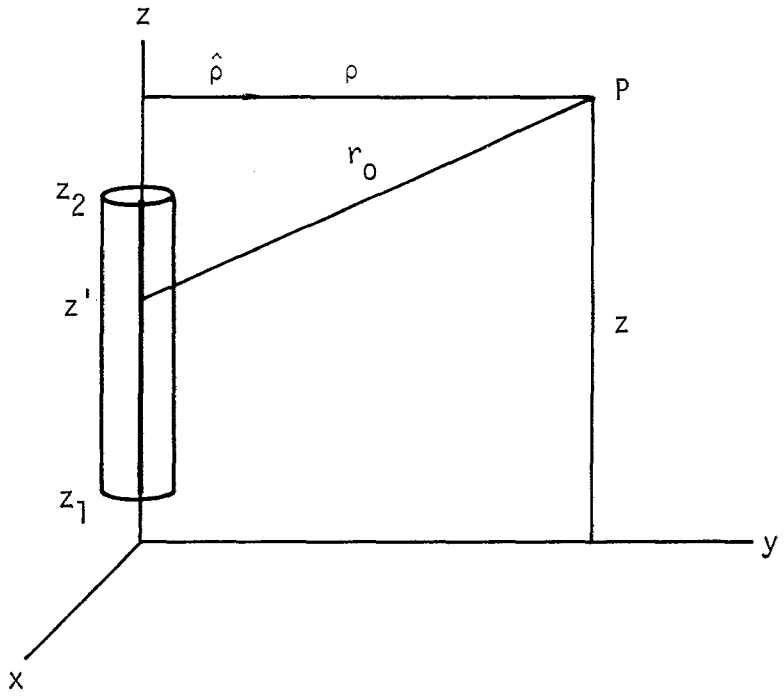

Figure A1. Current-Filament Geometry for the Thin-Wire Kernel.

$$E_\rho^f(\rho,z) = \frac{-j\eta}{2k^2\lambda\rho}\left[(z'-z)\ I\ \frac{\partial G_o}{\partial z'} + I\ G_o - (z'-z)\ G_o\ \frac{\partial I}{\partial z'}\right]_{z_1}^{z_2}, \tag{A5}$$

$$E_z^f(\rho,z) = \frac{j\eta}{2k^2\lambda}\left[G_o\ \frac{\partial I}{\partial z'} - I\ \frac{\partial G_o}{\partial z'}\right]_{z_1}^{z_2}. \tag{A6}$$

For a current that is constant over the length of the segment with strength I, the fields are

$$E_\rho^f(\rho,z) = \frac{I}{\lambda}\ \frac{j\eta}{2k^2}\left[\frac{\partial G_o}{\partial \rho}\right]_{z_1}^{z_2}, \tag{A7}$$

$$E_z^f(\rho,z) = -\frac{I}{\lambda}\ \frac{j\eta}{2k^2}\left\{\left[\frac{\partial G_o}{\partial z'}\right]_{z_1}^{z_2} + k^2\int_{z_1}^{z_2} G_o\ dz'\right\}. \tag{A8}$$

These field expressions are exact for the specified currents. The integral over z' of G_o is evaluated numerically in NEC.

Substituting sine and cosine currents and evaluating the derivatives yields the following equations for the fields. For

$$I = I_o \begin{pmatrix} \sin kz' \\ \cos kz' \end{pmatrix} , \tag{A9}$$

$$E_\rho^f(\rho,z) = \frac{-I_o}{\lambda} \frac{j\eta}{2k^2\rho} G_o \left\{ k(z-z') \begin{pmatrix} \cos kz' \\ -\sin kz' \end{pmatrix} \right. \tag{A10}$$

$$\left. + \left[1 - (z-z')^2 (1+jkr_o) \frac{1}{r_o^2} \right] \begin{pmatrix} \sin kz' \\ \cos kz' \end{pmatrix} \right\} \Bigg|_{z_1}^{z_2} ,$$

$$E_z^f(\rho,z) = \frac{I_o}{\lambda} \frac{j\eta}{2k^2} G_o \left\{ k \begin{pmatrix} \cos kz' \\ -\sin kz' \end{pmatrix} \right. \tag{A11}$$

$$\left. - (1+jkr_o)(z-z') \frac{1}{r_o^2} \begin{pmatrix} \sin kz' \\ \cos kz' \end{pmatrix} \right\} \Bigg|_{z_1}^{z_2} .$$

For a constant current of strength I_o,

$$E_\rho^f(\rho,z) = - \frac{I_o}{\lambda} \frac{j\eta\rho}{2k^2} \left[(1+jkr_o) \frac{G_o}{r_o^2} \right]_{z_1}^{z_2} , \tag{A12}$$

$$E_z^f(\rho,z) = - \frac{I_o}{\lambda} \frac{j\eta}{2k^2} \left\{ \left[(1+jkr_o)(z-z') \frac{G_o}{r_o^2} \right]_{z_1}^{z_2} \right. \tag{A13}$$

$$\left. + k^2 \int_{z_1}^{z_2} G_o \, dz' \right. .$$

Despite the seemingly crude approximation, the thin-wire kernel does accurately represent the effect of wire radius for wires that are sufficiently

thin. The accuracy range was studied by Poggio and Adams (ref. 11) where an extended thin-wire kernel was developed for wires that are too thick for the thin-wire approximation.

The derivation of the extended thin-wire kernel starts with the current on the surface of the source segment with surface density,

$$J(z') = I(z')/(2\pi a) \ ,$$

where a is the radius of the source segment. The geometry for evaluation of the fields is shown in figure A2. A current filament of strength $Id\phi/(2\pi)$ is integrated over ϕ with

$$\rho' = [\rho^2 + a^2 - 2a\rho \cos \phi]^{1/2} \ , \tag{A14}$$

$$r = [\rho'^2 + (z-z')^2]^{1/2} \ . \tag{A15}$$

Thus, the z component of the field of the current tube is

$$E_z^t(\rho,z) = \frac{1}{2\pi} \int_o^{2\pi} E_z^f(\rho',z)d\phi \ . \tag{A16}$$

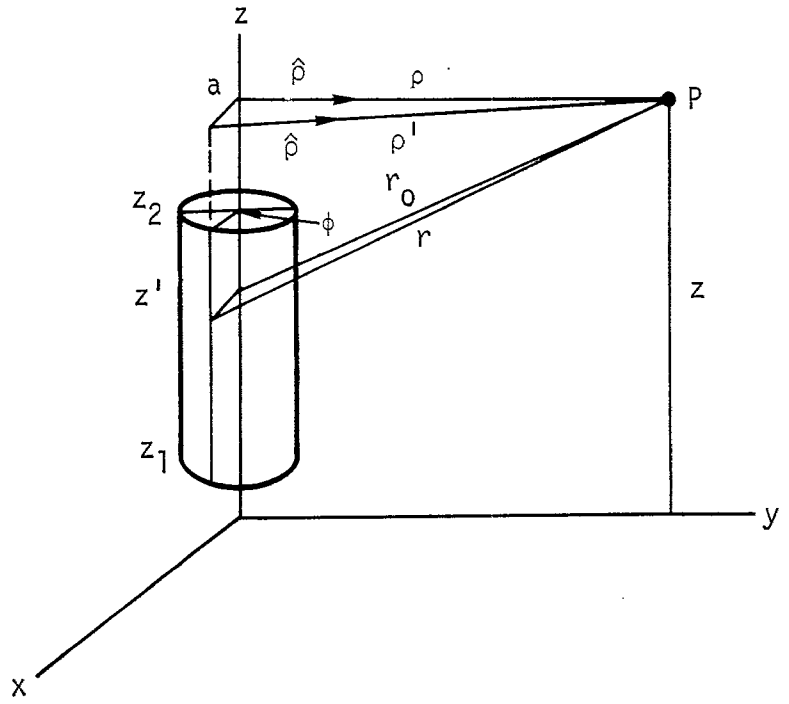

Figure A2. Current Geometry for the Extended Thin-Wire Kernel.

For the ρ component of field, the change in the direction of $\hat{\rho}'$ must be considered. The field in the direction $\hat{\rho}$ is

$$E_z^t(\rho,z) = \frac{1}{2\pi}\int_o^{2\pi} E_\rho^f(\rho',z)(\hat{\rho}\cdot\hat{\rho}')d\phi \ , \tag{A17}$$

where

$$\hat{\rho}\cdot\hat{\rho}' = \frac{\rho - a\cos\phi}{\rho'} = \frac{\partial\rho'}{\partial\rho}$$

The integrals over ϕ in equations (A16) and (A17) cannot be evaluated in closed form. Poggio and Adams, however, have evaluated them as a series in powers of a^2 (ref. 11). The first term in the series gives the thin-wire kernel. For the extended thin-wire kernel, the second term involving a^2 is retained with terms of order a^4 neglected. As with the thin-wire kernel, the field observation point is on the segment surface. Hence, when evaluating the field on the source segment, $\rho = a$.

The field equations with the extended thin-wire approximation are given below. For a sinusoidal current of equation (A4),

$$E_\rho(\rho,z) = \frac{-j\eta}{2k^2\lambda\rho}\left[(z'-z)I\frac{\partial G_2}{\partial z'} + IG_2 - (z'-z)G_2\frac{\partial I}{\partial z'}\right]_{z_1}^{z_2} , \tag{A18}$$

$$E_z(\rho,z) = \frac{j\eta}{2k^2\lambda}\left[G_1\frac{\partial I}{\partial z'} - I\frac{\partial G_1}{\partial z'}\right]_{z_1}^{z_2} , \tag{A19}$$

For a constant current of strength I_o,

$$E_\rho(\rho,z) = \frac{I}{\lambda}\frac{j\eta}{2k^2}\left[\frac{\partial G_1}{\partial \rho}\right]_{z_1}^{z_2}, \tag{A20}$$

$$E_z(\rho,z) = -\frac{I}{\lambda}\frac{j\eta}{2k^2}\left\{\left[\frac{\partial G_1}{\partial z'}\right]_{z_1}^{z_2} + k^2\left[1-\frac{(ka)^2}{4}\right]\int_{z_1}^{z_2} G_o\,dz' - \frac{(ka)^2}{4}\left[\frac{\partial G_o}{\partial z'}\right]_{z_1}^{z_2}\right\}. \tag{A21}$$

The term G_1 is the series approximation of

$$G_1^t = \frac{1}{2\pi}\int_o^{2\pi} G\,d\phi, \tag{A22}$$

where

$$G = \exp(-jkr)/r.$$

Neglecting terms of order a^4,

$$G_1 = G_o\left\{1 - \frac{a^2}{2r_o^2}(1+jkr_o) + \frac{a^2\rho^2}{4r_o^4}\left[3(1+jkr_o) - k^2r_o^2\right]\right\}, \tag{A23}$$

$$\frac{\partial G_1}{\partial z'} = \frac{(z-z')}{r_o^2}G_o\left\{(1+jkr_o) - \frac{a^2}{2r_o^2}\left[3(1+jkr_o) - k^2r_o^2\right] - \frac{a^2\rho^2}{4r_o^4}\left[jk^3r_o^3 + 6k^2r_o^2 - 15(1+jkr_o)\right]\right\}, \tag{A24}$$

$$\frac{\partial G_1}{\partial \rho} = -\frac{\rho G_o}{r_o^2}\left\{(1+jkr_o) - \frac{a^2}{r_o^2}\left[3(1+jkr_o) - k^2r_o^2\right]\right.$$

$$\left. - \frac{a^2\rho^2}{4r_o^4}\left[jk^3r_o^3 + 6k^2r_o^2 - 15(1+jkr_o)\right]\right\} . \tag{A25}$$

The term G_2 is the series approximation of

$$G_2^t = \frac{1}{2\pi}\int_o^{2\pi} \frac{\rho - a\cos\phi}{\rho'^2} G\, d\phi . \tag{A26}$$

To order a^2,

$$G_2 = \frac{G_o}{\rho}\left\{1 + \frac{a^2\rho^2}{4r_o^4}\left[3(1+jkr_o) - k^2r_o^2\right]\right\} , \tag{A27}$$

$$\frac{\partial G_2}{\partial z'} = \frac{(z-z')}{\rho r_o^2} G_o \left\{(1+jkr_o) - \frac{a^2\rho^2}{4r_o^4}\left[jk^3r_o^3 + 6k^2r_o^2 - 15(1+jkr_o)\right]\right\} . \tag{A28}$$

Equation (A20) makes use of the relation

$$(\hat{\rho}\cdot\hat{\rho}')\frac{\partial G}{\partial \rho'} = \frac{\partial G}{\partial \rho'}\frac{\partial \rho'}{\partial \rho} = \frac{\partial G}{\partial \rho} , \tag{A29}$$

while equation (A21) follows from

$$G_1 = \left[1 - \frac{(ka)^2}{4} - \frac{a^2}{4}\frac{\partial^2}{\partial z'^2}\right] G_o . \tag{A30}$$

When the observation point is within the wire ($\rho<a$), a series expansion in ρ rather than a is used for G_o and G_2. For G_1 this simply involves interchanging ρ and a in equations (A23) and (A24). Then for $\rho \leq a$, with

$$r_a = \left[a^2 + (z-z')^2\right]^{1/2} , \tag{A31}$$

$$G_a = \exp(-jkr_a)/r_a \ , \tag{A32}$$

the expressions for G_1, G_2 and their derivatives are

$$G_1 = G_a \left\{ 1 - \frac{\rho^2}{2r_a^2}(1+jkr_a) + \frac{a^2\rho^2}{4r_a^4}\left[3(1+jkr_a) - k^2r_a^2\right] \right\} \ , \tag{A33}$$

$$\frac{\partial G_1}{\partial z'} = \frac{(z-z')}{r_a^2} G_a \left\{ (1+jkr_a) - \frac{\rho^2}{2r_a^2}\left[3(1+jkr_a) - k^2r_a^2\right] - \frac{a^2\rho^2}{4r_a^4}\left[jk^3r_a^3 + 6k^2r_a^2 - 15(1+jkr_a)\right] \right\} \ , \tag{A34}$$

$$\frac{\partial G_1}{\partial \rho} = -\frac{\rho}{r_a^2} G_a \left\{ (1+jkr_a) - \frac{a^2}{2r_a^2}\left[3(1+jkr_a) - k^2r_a^2\right] \right\} \ , \tag{A35}$$

$$G_2 = -\frac{\rho}{2r_a^2} G_a \ (1+jkr_a) \ , \tag{A36}$$

$$\frac{\partial G_2}{\partial z'} = -\frac{(z-z')\rho}{2r_a^4} G_a \left[3(1+jkr_a) - k^2r_a^2\right] \ . \tag{A37}$$

Special treatment of bends in wires is required when the extended thin wire kernel is used. The problem stems from the cancellation of terms evaluated at z_1 and z_2 in the field equations when segments are part of a continuous wire. The current expansion in NEC results in a current having a continuous value and derivative along a wire without junctions. This ensures that for two adjacent segments on a straight wire, the contributions to the z component of electric field at z_2 of the first segment exactly cancel the contributions from z_1, representing the same point, for the second segment. For a straight wire of several segments, the only contributions to E_z with either the thin-wire or extended thin-wire kernel come from the two wire ends and the integral of G_o along the wire. For the ρ component of field or either component at a bend, while there is not complete cancellation, there may be partial cancellation of large end contributions.

The cancellation of end terms makes necessary a consistent treatment of the current on both sides of a bend for accurate evaluation of the field. This is easily accomplished with the thin-wire kernel since the current filament on the wire axis is physically continuous around a bend. However, the current tube assumed for the extended thin-wire kernel cannot be continuous around its complete circumference at a bend. This was found to reduce the solution accuracy when the extended thin-wire kernel was used for bent wires.

To avoid this problem in NEC, the thin-wire form of the end terms in equations (A5) through (A8) are always used at a bend or change in radius. The extended thin-wire kernel is used only at segment ends where two parallel segments join, or at free ends. The switch from extended thin-wire form to the thin-wire form is made from one end of a segment to the other rather than between segments where the cancellation of terms is critical.

When segments are separated by a large distance, the interaction may be computed with sufficient accuracy by treating the segment current as an infinitesimal current element at the segment center. In spherical coordinates, with the segment at the origin along the $\Theta = 0$ axis, the electric field is

$$E_r(r,\Theta) = \frac{M\eta}{2\pi r^2} \exp(-jkr)\left(1 - \frac{j}{kr}\right) \cos\Theta \ ,$$

$$E_\Theta(r,\Theta) = \frac{M\eta}{4\pi r^2} \exp(-jkr)\left(1+jkr - \frac{j}{kr}\right) \sin\Theta \ .$$

The dipole moment M for a constant current I on a segment of length Δ_i is

$$M = I\ \Delta_i \ .$$

For a current $I \cos[k(s - s_i)]$ with $|s - s_i| < \Delta_i/2$,

$$M = \frac{2I}{k} \sin(k\Delta_i/2) \ ,$$

while for a current $I \sin[k(s - s_i)]$,

$$M = 0 \ .$$

Use of this approximation saves a significant amount of time in evaluating the interaction matrix elements for large structures. The minimum interaction distance at which it is used is selected by the user in NEC. A default distance of one wavelength is set, however.

For each of the three methods of computing the field at a segment due to the current on another segment, the field is evaluated on the surface of the observation segment. Rather than choosing a fixed point on the segment surface, the field is evaluated at the cylindrical coordinates ρ', z with the source segment at the origin. If the center point on the axis of the observation segment is at ρ, z, then

$$\rho' = \left[\rho^2 + a_o^2\right]^{1/2} ,$$

where a_o is the radius of the observation segment. Also, the component of E_ρ tangent to the observation segment is computed as

$$\vec{E}_\rho \cdot \hat{s} = (\hat{\rho}\cdot\hat{s}) \frac{\rho}{\rho'} E_\rho .$$

Inclusion of the factor ρ/ρ', which is the cosine of the angle between $\hat{\rho}$ and $\hat{\rho}'$, is necessary for accurate results at bends in thick wires.

☆ U.S. GOVERNMENT PRINTING OFFICE: 1979-680-647-524